European Radiology

Value of 3-T MR imaging in intraductal papillary mucinous neoplasm with a concomitant invasive carcinoma

--Manuscript Draft--

Manuscript Number:	EURA-D-22-00800R1
Full Title:	Value of 3-T MR imaging in intraductal papillary mucinous neoplasm with a concomitant invasive carcinoma
Article Type:	Original Article
Funding Information:	
Abstract:	Objectives: To examine the value of 3-T MRI for evaluating the difference between the pancreatic parenchyma of intraductal papillary mucinous neoplasm with a concomitant invasive carcinoma (IPMN-IC) and the pancreatic parenchyma of patients without an IPMN-IC.Methods: A total of 132 patients who underwent abdominal 3-T MRI. Of the normal pancreatic parenchymal measurements, the pancreas-to-muscle signal intensity ratio in in-phase imaging (SIR-I), SIR in opposed-phase imaging (SIR-O), SIR in T2-weighted imaging (SIR-T2), ADC (×10-3 mm2/s) in DWI, and proton density fat fraction (PDFF [%]) in multi-echo 3D DIXON were calculated. The patients were divided into three groups (normal pancreas group: n = 60, intraductal papillary mucinous neoplasm (IPMN) group: n = 60, IPMN-IC group: n = 12).Results: No significant differences were observed among the three groups in age, sex, body mass index, prevalence of diabetes mellitus, and hemoglobin A1c ($p = 0.141$ to $p = 0.657$). In comparisons among the three groups, the PDFF showed a significant difference ($p < 0.001$), and there were no significant differences among the three groups in SIR-I, SIR-O, SIR-T2, and ADC ($p = 0.153$ to $p = 0.684$). The PDFF of the pancreas was significantly higher in the IPMN-IC group than in the normal pancreas group or the IPMN group ($p < 0.001$ and $p < 0.001$, respectively), with no significant difference between the normal pancreas group and the IPMN group ($p = 0.916$).Conclusions: These observations suggest that the PDFF of the pancreas is associated with the presence of IPMN-IC.
Corresponding Author:	Hidemitsu Sotozono Kawasaki Medical School Kurashiki, Okayama JAPAN
Corresponding Author Secondary Information:	
Corresponding Author's Institution:	Kawasaki Medical School
Corresponding Author's Secondary Institution:	
First Author:	Hidemitsu Sotozono
First Author Secondary Information:	
Order of Authors:	Hidemitsu Sotozono
	Akihiko Kanki
	Kazuya Yasokawa
	Akira Yamamoto
	Hiroyasu Sanai
	Kazunori Moriya
	Tsutomu Tamada
Order of Authors Secondary Information:	
Author Comments:	We are resubmitting our paper “Value of 3-T MR imaging in intraductal papillary mucinous neoplasm with a concomitant invasive carcinoma” (Original Research) through on-line submission system.

	My colleagues and I wish to thank you for your consideration.

Responses to Comments from the Reviewer

Reviewer #1

This is an interesting and well-written paper. The prominent finding is relevant: IPMN with concomitant invasive carcinoma was associated with high pancreatic fat content, as compared to both a normal group and an IPMN group. The Authors accepted the changes suggested by the Reviewers. The new title is appropriate. The overall quality has been significantly improved. Consider adding a couple of sentences in the Discussion section regarding the role of "high-risk stigmata" and "worrisome features" (Fukuoka consensus guidelines).

Response: As suggested, we have added text about the role of "high-risk stigmata" and "worrisome features" in the Discussion section.

Value of 3-T MR imaging in intraductal papillary mucinous neoplasm with a concomitant invasive carcinoma

Hidemitsu Sotozono*, Akihiko Kanki, Kazuya Yasokawa, Akira Yamamoto, Hiroyasu Sanai, Kazunori Moriya, Tsutomu Tamada

Department of Radiology, Kawasaki Medical School, Kurashiki, Japan.

*Address reprint requests to: H.S., Department of Radiology, Kawasaki Medical School, 577 Matsushima, Kurashiki city, Okayama, 701-0192, Japan

E-mail: sotozono@med.kawasaki-m.ac.jp

Telephone number: 81-86-462-1111

Fax number: 81-86-462-1199

Value of 3-T MR imaging in intraductal papillary mucinous neoplasm with a concomitant invasive carcinoma

Abstract

Objectives: To examine the value of 3-T MRI for evaluating the difference between the pancreatic parenchyma of intraductal papillary mucinous neoplasm with a concomitant invasive carcinoma (IPMN-IC) and the pancreatic parenchyma of patients without an IPMN-IC.

Methods: A total of 132 patients who underwent abdominal 3-T MRI. Of the normal pancreatic parenchymal measurements, the pancreas-to-muscle signal intensity ratio in in-phase imaging (SIR-I), SIR in opposed-phase imaging (SIR-O), SIR in T2-weighted imaging (SIR-T2), ADC ($\times 10^{-3}$ mm^2/s) in DWI, and proton density fat fraction (PDFF [%]) in multi-echo 3D DIXON were calculated. The patients were divided into three groups (normal pancreas group: n = 60, intraductal papillary mucinous neoplasm (IPMN) group: n = 60, IPMN-IC group: n = 12).

Results: No significant differences were observed among the three groups in age, sex, body mass index, prevalence of diabetes mellitus, and hemoglobin A1c ($p = 0.141$ to $p = 0.657$). In comparisons among the three groups, the PDFF showed a significant difference ($p < 0.001$), and there were no significant differences among the three groups in SIR-I, SIR-O, SIR-T2, and ADC ($p = 0.153$ to $p = 0.684$). The PDFF of the pancreas

was significantly higher in the IPMN-IC group than in the normal pancreas group or the IPMN group ($p < 0.001$ and $p < 0.001$, respectively), with no significant difference between the normal pancreas group and the IPMN group ($p = 0.916$).

Conclusions: These observations suggest that the PDFF of the pancreas is associated with the presence of IPMN-IC.

Key words: Pancreas; MR cholangiopancreatography (MRCP); intraductal papillary mucinous neoplasm (IPMN); proton density fat fraction (PDFF); pancreatic ductal adenocarcinoma (PDAC)

Key points:

- The cause and risk factors of IPMN with a concomitant invasive carcinoma have not yet been clarified.
- The PDFF of the pancreas was significantly higher in the IPMN-IC group than in the normal pancreas group or the IPMN group.
- Pancreatic PDFF may be a potential biomarker for the development of IPMN with a concomitant invasive carcinoma.

Abbreviations and acronyms

BMI: Body mass index

DM: Diabetes mellitus

FOV: Field of view

HbA1c: Hemoglobin A1c

IPMN: Intraductal papillary mucinous neoplasm

IPMN-IC: Intraductal papillary mucinous neoplasm with a concomitant invasive carcinoma

PACS: Picture Archiving and Communication System

PDAC: Pancreatic ductal adenocarcinoma

PDFF: Proton density fat fraction

SIR: Signal intensity ratio

SIR-I: Signal intensity ratio in in-phase imaging

SIR-O: Signal intensity ratio in opposed-phase imaging

SIR-T2: Signal intensity ratio in T2-weighted imaging

T1WI: T1-weighted imaging

T2WI: T2-weighted imaging

TE: Echo time

TR: Repetition time

TSE: Turbo spin echo

Introduction

Intraductal papillary mucinous neoplasm (IPMN) is characterized by an expansion of the main pancreatic duct or a branch due to a papillary growth of the epithelium, with rich mucin production. The IPMN is a precursor of pancreatic ductal adenocarcinoma (PDAC) caused by the papillary proliferation of the epithelium (1-10). There are two types of IPMN-related pancreatic carcinoma, one in which the IPMN itself becomes malignant (IPMN with associated invasive carcinoma) and the other in which pancreatic cancer develops in a site distant from the IPMN (IPMN with a concomitant invasive carcinoma: IPMN-IC) (2, 4-6, 8-13). It is often difficult to distinguish between IPMN with associated invasive carcinoma and IPMN-IC, but special attention should be paid to the appearance of IPMN-IC, which causes pancreatic cancer at a site distant from the IPMN (14). Regarding the risk of developing IPMN with associated invasive carcinoma, the findings of "high-risk stigmata" and "worrisome features" were proposed by the international consensus guidelines for the management of IPMN and mucinous cystic neoplasm of the pancreas (15). On the other hand, the cause of IPMN-IC and its risk factors have not yet been clarified. If the risk factors that cause IPMN-IC can be elucidated on radiological images, it would lead to early detection of pancreatic cancer, which would be very useful clinically. Recent reports suggest that pancreatic

fatty infiltration is a risk factor for conventional PDAC (16-23). Pancreatic fatty infiltration induces chronic inflammation caused by the release of various cytokines and chemokines by adipose tissue, leading to the development of pancreatic cancer. Therefore, in this study, the proton density fat fraction (PDFF) was included among the pancreatic parenchymal measurements. The purpose of this study was to clarify the quantitative magnetic resonance imaging (MRI) indices associated with IPMN-IC using 3-T MRI.

Materials and Methods

Patients

The Institutional Review Board approved this retrospective study and waived the requirement for informed consent. Patient selection and the collection of clinical data were performed by the study coordinator (**). From January 2017 to December 2020, 12 patients who were histologically diagnosed with IPMN-IC underwent abdominal MRI including MR cholangiopancreatography (MRCP) and multi-echo 3D DIXON using 3-T MRI (IPMN-IC group). The location of the tumor was in the head of the pancreas in 4 (33.3%), in the body in 3 (25%), and in the tail in 5 (41.7%). All IPMN-ICs were branch duct type. Next, the study coordinator selected patients with matching

clinical data including age, sex, body mass index (BMI [kg/m^2]), hemoglobin A1c (HbA1c), and the presence or absence of diabetes mellitus (DM) for comparison with the IPMN-IC group. The presence of DM was defined as HbA1c ≥ 6.5% and/or treatment for DM. As a result, 60 consecutive patients without pancreatic disease (normal pancreas group) and 60 consecutive patients with IPMN and no invasive carcinoma (IPMN group) were selected using medical record and MRI findings within the same period. These patients also underwent the same abdominal MRI examinations as the IPMN-IC group. There were no significant differences in age, sex, BMI, HbA1c, and presence or absence of DM among the normal pancreas group, IPMN group, and IPMN-IC group. Finally, a total of 132 patients were analyzed in this study. A normal pancreas was defined as no obvious cysts or neoplastic lesions on MRI. IPMN was defined as branch duct dilatation (≥ 5 mm) communicating with the main pancreatic duct on MRI (15). Sixty patients in the IPMN group were followed up by ultrasonography, CT, and MRI for an average of 37.2 months (1-61 months), and only one of them was clinically diagnosed with IPMN with associated invasive carcinoma. Cases diagnosed with IPMN-IC were not included in the IPMN group. Twelve IPMN-ICs were defined as histologically proven PDAC by surgically resected specimens in 8 lesions or pancreatic biopsy using endoscopic ultrasonography in 4 lesions. Of 11

IPMN-ICs, PDAC was obviously distant from the IPMN lesion according to the MRCP images. The remaining one IPMN-IC in which PDAC was close to the IPMN lesion on MRCP images was found to lack the transition of IPMN to PDAC.

Imaging techniques

MRI was performed under fasting conditions (3 hours) using a 3-T scanner (Ingenia 3-T CX Quasar Dual; Philips Medical Systems) with a 32-channel phased-array coil (n = 108; normal group 53, IPMN group 48, IPMN-IC group 7), a 3-T scanner (Vantage Titan 3-T; Canon Medical Systems) with a 16-channel phased-array coil (n = 20; normal group 7, IPMN group 12, IPMN-IC group 1) or a 3-T scanner (Ingenia Elition; Philips Medical Systems) with a 32-channel phased-array coil (n = 4; IPMN-IC group 4). The MRI examinations included axial in-phase and opposed-phase imaging, axial T2-weighted imaging (T2WI), axial diffusion-weighted imaging (DWI), multi-echo 3D DIXON, and MRCP.

Ingenia 3-T CX Quasar Dual

The following were acquired: 3D T1W mDIXON axial in-phase and opposed-phase imaging (repetition time [TR], 3.2 ms; echo time [TE], 2.0 and 1.14 ms; matrix, 224 × 192; bandwidth, 1992.8 Hz per pixel; field of view [FOV], 350 × 300 mm^2; flip angle, 10°; acquisition time, 18.5 s; slice thickness, 3 mm; no interslice gap; parallel imaging

factor, 2.3); axial turbo spin echo (TSE) T2WI (TR, 1346 ms [respiratory trigger]; TE, 80 ms; matrix, 320 × 320; bandwidth, 1531.9 Hz per pixel; FOV, 350 × 350 mm^2; flip angle, 90°; acquisition time, 2 min 33 s [respiratory trigger]; slice thickness, 6 mm; interslice gap, 1 mm; parallel imaging factor, 2.3); axial single-shot spin echo echo-planar DWI (TR, 1203 ms [respiratory trigger]; TE, 70 ms; matrix, 128 × 106; bandwidth, 2421.4 Hz per pixel; FOV, 350 × 295 mm^2; flip angle, 90°; acquisition time, 2 min 6 s [respiratory trigger]; slice thickness, 6 mm; interslice gap, 1 mm; parallel imaging factor, 2; b-values, 0 and 800 s/mm^2); and multi-echo 3D DIXON (3D mDIXON quant) (TR, 5.9 ms; TE, 1.02 ms; ΔTE, 0.7 ms; matrix, 144 × 106; bandwidth, 2515.7 Hz per pixel; FOV, 350 × 350 mm^2; flip angle, 3°; acquisition time, 15.4 s; slice thickness, 3 mm; no interslice gap; parallel imaging factor, 2 [phase]: 1.2 [slice]). Apparent diffusion coefficient (ADC) maps were calculated for a pair of b-values (0 and 800 s/mm^2) by mono exponential fitting. Parametric PDFF maps were automatically generated on the imager software from the 6 echo mDIXON examination. MRCP (TR, 2007 ms [respiratory trigger]; TE, 600 ms; matrix, 336 × 336; bandwidth, 375.8 Hz per pixel; FOV, 300 × 300 mm^2; flip angle, 90°; acquisition time, 2 min 27 s [respiratory trigger]; slice thickness, 2 mm; no interslice gap; compressed sensing, 5) was also acquired.

3-T MR scanner with Vantage Titan 3T; Canon

The following were acquired: T1W dual echo axial in-phase and opposed-phase imaging (TR, 160 ms; TE, 1.3 and 2.6 ms; matrix, 320 × 224; bandwidth, 781 Hz per pixel; FOV, 350 × 350 mm^2; flip angle, 60°; acquisition time, 19 s; slice thickness, 6 mm; interslice gap, 1 mm; parallel imaging factor, 2); axial fast spin-echo T2WI (TR, 3000 ms; TE, 75 ms; matrix, 320 × 224; bandwidth, 325.5 Hz per pixel; FOV, 350 × 350 mm^2; flip angle, 90°; acquisition time, 42 s; slice thickness, 6 mm; interslice gap, 1 mm; parallel imaging factor, 2.5); axial single-shot spin echo echo-planar DWI (TR, 6000 ms; TE, 69 ms; matrix, 144 × 128; bandwidth, 1953.1 Hz per pixel; FOV, 350 × 350 mm^2; flip angle, 90°; acquisition time, 3 min 36 s; slice thickness, 6 mm; interslice gap, 1 mm; parallel imaging factor, 3; b-values, 0 and 800 s/mm^2); and multi-echo 3D DIXON (2 point DIXON) (TR, 5.1 ms; TE, 1.1 and 2.8 ms; matrix, 208 × 160; bandwidth, 1302 Hz per pixel; FOV, 350 × 350 mm^2; flip angle, 12°; acquisition time, 18 s; slice thickness, 5 mm; no interslice gap; parallel imaging factor, 2). ADC maps were calculated for a pair of b-values (0 and 800 s/mm^2) by mono exponential fitting. Parametric PDFF maps were automatically generated on the imager software from the 2 echo DIXON examination. MRCP (TR, 3649 ms [respiratory trigger]; TE, 494 ms; matrix, 352 × 320; bandwidth, 488 Hz per pixel; FOV, 300 × 300 mm^2; flip angle, 90°;

acquisition time, 3 min 21 s [respiratory trigger]; slice thickness, 2 mm; no interslice gap; parallel imaging factor, 3) was also acquired.

Ingenia Elition 3.0T

The following were acquired: 3D T1W mDIXON axial in-phase and opposed-phase imaging (TR, 3.5 ms; TE, 2.3 and 1.14 ms; matrix, 224 × 192; bandwidth, 1487.9 Hz per pixel; FOV, 350 × 350 mm^2; flip angle, 10°; acquisition time, 21 s; slice thickness, 3 mm; no interslice gap; parallel imaging factor, 2.3); axial TSE T2WI (TR, 1685 ms [respiratory trigger]; TE, 80 ms; matrix, 320 × 320; bandwidth, 1347 Hz per pixel; FOV, 350 × 350 mm^2; flip angle, 90°; acquisition time, 3 min 9 s [respiratory trigger]; slice thickness, 6 mm; interslice gap, 1 mm; parallel imaging factor, 2); axial single-shot spin echo echo-planar DWI (TR, 1195 ms [respiratory trigger]; TE, 69 ms; matrix, 128 × 128; bandwidth, 2290.8 Hz per pixel; FOV, 350 × 295 mm^2; flip angle, 90°; acquisition time, 4 min 12 s [respiratory trigger]; slice thickness, 3.5 mm; no interslice gap; parallel imaging factor, 2; b-values, 0 and 800 s/mm^2); and multi-echo 3D DIXON (3D mDIXON quant) (TR, 5.7 ms; TE, 0.98 ms; ΔTE, 0.7 ms; matrix, 144 × 118; bandwidth, 2314.8 Hz per pixel; FOV, 350×350 mm^2; flip angle, 3°; acquisition time, 15 s; slice thickness, 3 mm; no interslice gap; parallel imaging factor, 2 [phase]: 1.2 [slice]). ADC maps were calculated for a pair of b-values (0 and 800 s/mm^2) by mono

exponential fitting. Parametric PDFF maps were automatically generated on the imager software from the 6 echo mDIXON examination. MRCP (TR, 2007 ms [respiratory trigger]; TE, 600 ms; matrix, 336 × 336; bandwidth, 375.8 Hz per pixel; FOV, 300 × 300 mm^2; flip angle, 90°; acquisition time, 2 min 27 s [respiratory trigger]; slice thickness, 2 mm; no interslice gap; compressed sensing, 5) was also acquired.

Image analysis

The image analysis was performed by two fellowship-trained radiologists with 7 years and 15 years of experience in abdominal MRI (** and **, respectively) in consensus. Of the normal pancreatic parenchymal measurements, the pancreas-to-muscle (erector spinae muscles) signal intensity ratio (SIR) on in-phase imaging (SIR-I = pancreas SI on in-phase/SI of erector spinae muscle on in-phase), the SIR on opposed-phase imaging (SIR-O = pancreas SI on opposed-phase/SI of erector spinae muscle on opposed-phase), the SIR on T2WI (SIR-T2 = pancreas SI on T2WI/SI of erector spinae muscle on T2WI), the ADC on the ADC map ($\times 10^{-3}$ mm^2/s), and the PDFF (%) were calculated using the region of interest (ROI) placement technique. MRI measurements were manually performed on a standard picture archiving and communication system (PACS) (Synapse; Fujifilm). Measurements of the ROI were taken in the head of the pancreas in the normal pancreas group and the IPMN group (Figs. 1, 2). In the IPMN-

IC group, the ROI of the normal pancreas region was set downstream of the tumor to avoid the effect of the tumor on the pancreatic parenchyma (Fig. 3). The radiologists carefully drew the ROI as a circle or oval as large as possible in a homogeneous region of the pancreatic parenchyma, avoiding the pancreatic duct, vessels, retroperitoneal fat, and artifacts. An ROI was placed on the erector spinae muscle in a region that showed uniform signal intensity on either the left or right side with reference to T2WI. The ROI placements of pancreatic parenchyma and erector spinae muscle in each patient were carefully performed to be as co-located as possible between sequences using five MR sequences including in-phase T1WI, opposed-phase T1WI, T2WI, ADC map, and parametric PDFF map aligned on the PACS monitor.

Statistical analysis

The quantitative MRI indices and clinical data were compared using Kruskal-Wallis, χ^2, and Mann-Whitney U tests. The Kruskal-Wallis test and the χ^2 test were used to compare differences among the three groups. If a significant difference was found, the two relevant groups were further compared using the χ^2 test and the Mann-Whitney test. Data were analyzed using SPSS for Windows v24.0 software (SPSS, Chicago, IL). A *p* value less than 0.05 was taken to indicate significance.

Results

All quantitative MRI indices using ROI placement technique were successfully calculated for all 12 patients with IPMN-IC, 60 patients with normal pancreas, and 60 patients with IPMN. Table 1 shows the comparison of the patients' clinical characteristics among the three groups. The PDFF showed a significant difference ($p < 0.001$), and there were no significant differences among the three groups in SIR-I, SIR-O, SIR-T2, and ADC ($p = 0.423$, $p = 0.153$, $p = 0.348$, and $p = 0.684$, respectively). Table 2 shows the comparison of the quantitative MRI indices among the three groups. Indeed, only slight overlap was seen between the PDFF of the IPMN-IC group and the normal pancreas group or the IPMN-IC group and the IPMN group (Fig. 4). The PDFF of the pancreas was significantly higher in the IPMN-IC group than in the normal pancreas group or the IPMN group ($p < 0.001$ and $p < 0.001$, respectively), and there was no significant difference between the normal pancreas group and the IPMN group ($p = 0.916$).

Discussion

Using surgically resected samples or pancreatic biopsies as the pathological reference standard, quantitative indices of pancreatic parenchyma were compared using 3-T MRI

among three groups (normal pancreas group, IPMN group, and IPMN-IC group), with matching clinical features of age, sex, BMI, and DM. The present study is the first to evaluate the risk factors for carcinogenesis of IPMN-IC using MRI.

IPMNs progress from adenomas to carcinomas. It is known that there are two types of IPMN-related pancreatic carcinomas, IPMN with associated invasive carcinoma and IPMN-IC (2, 4, 5, 11, 12). IPMN with associated invasive carcinoma is better known than before, and the international consensus guidelines for management of IPMN and mucinous cystic neoplasm of the pancreas are used to address the risk factors for carcinogenesis. Although the “high-risk stigmata” and “worrisome features” proposed in the Fukuoka guidelines are very useful in predicting IPMN with associated invasive carcinoma and high-grade dysplasia, the risk factors for IPMN-IC have not yet been clarified (15). In 2002, Yamaguchi et al. reported the clinicopathologic findings of 7 Japanese patients with IPMN-IC first (6). Since then, cases of IPMN-IC have been reported mainly from Japan, with a frequency of 4% to 10% of resected IPMNs (6, 7, 9). The clinical outcome of patients with IPMN-IC is better than that of conventional PDAC patients, because IPMN-IC is diagnosed earlier than conventional PDAC due to the opportunity for clinical detection of IPMN, or because the clinicopathological features of IPMN-derived PDAC are different from those of conventional PDAC (4).

Murakami et al. showed that the overall 5-year survival rates of patients with IPMN-derived PDAC were significantly higher than those of patients with conventional PDAC (24). In other words, by recognizing the risk factors for carcinogenesis and detecting them earlier, it is expected that the prognosis will be further improved. Previous studies identified the following predictors of PDAC associated with IPMN: age > 70 years, elevated serum carbohydrate antigen 19-9 levels, worsening DM, gastric IPMN without *GNAS* gene mutations, or multifocal cysts (11, 14, 25, 26). In contrast, other studies have previously reported that there are no imaging and morphological features of IPMN that predict IPMN-IC (10, 13). In the present study, the pancreatic PDFF with multi-echo 3D DIXON, which is a quantitative index of pancreatic steatosis using MRI (16, 27-30), was significantly higher in the IPMN-IC group than in the normal pancreas or IPMN group, and there was no significant difference between the normal pancreas and IPMN groups. In addition, no association was observed between other MRI quantitative indices of the pancreas including SIR-I, SIR-O, SIR-T2, and ADC and the incidence of IPMN-IC. Pancreatic adipose infiltration, or replacement of normal pancreatic tissue with adipose tissue, has been demonstrated to be associated with obesity, DM, old age, metabolic factors, and non-alcoholic fatty liver disease (16, 31). In addition, recent reports suggest that pancreatic fat infiltration is a risk factor for PDAC (16-23).

Pancreatic fat infiltration induces chronic inflammation caused by the release of pro-inflammatory adipokines/cytokines, such as leptin and monocyte chemotactic protein-1, by adipose tissue, leading to the development of PDAC (23). Fukui et al. showed that MRI-PDFF was correlated with the histological pancreatic fat fraction, demonstrating that MRI-PDFF was higher in the PDAC group than in the control group (16). In addition, they reported that MRI-PDFF was the only independent risk factor for PDAC on multivariate analysis (16). Kashiwagi et al. reported that IPMN cases had significantly higher fat content than cases without IPMN (1). The present results showed no significant difference in fat content between the IPMN group and the normal pancreas group. The difference in results between those studies may be due to the fact that Kashiwagi et al. used CT, since the MR multi-echo 3D DIXON is superior to CT in quantifying fat degeneration (32). In particular, CT, which offers a semi-quantitative approach, has less accuracy in detecting mild degrees of steatosis, whereas the sensitivity and specificity of multi-echo 3D DIXON in detecting histologic steatosis were 95.0% and 100%, respectively (33, 34). Thus, given that the PDFF was significantly higher in the IPMN-IC group than in the normal pancreas or IPMN group, it is possible that an increase in fat content in IPMN causes the occurrence of IPMN with a concomitant invasive carcinoma.

This study has some limitations. First, it was a retrospective, single-center study with a small number of patients with IPMN-IC. However, the present study is the first to evaluate the carcinogenetic risk factors for IPMN-IC using MRI. In the future, it will be necessary to confirm the present results in prospective, multicenter, clinical trials with a larger number of patients. Second, since the present study was performed using three 3-T MR scanners from two different vendors, there may be an error in the MR quantitative indices between the scanners. However, semi-quantitative MR indices such as SIR-I, SIR-O, and SIR-T2 SI, and ADC values using the same b-values among scanners may have minimal error. In addition, recent studies reported that estimation of the PDFF with hepatic MRI using multipoint DIXON techniques is highly reproducible across field strengths and vendors (35, 36). One scanner was a 2-point Dixon, whereas the two other scanners were 6-point Dixon. It is generally known that the accuracy of PDFF is reduced with 2-point Dixon due to the T1 bias, the effect of T2* signal decay due to iron deposition, and the inability to consider the multi-peak of fat (34). However, the effects of iron deposition on the pancreas are thought to be small. Third, pancreatic fat infiltration is sometimes heterogeneous, and the measured location of the pancreas may not represent the full spectrum of pancreatic fat infiltration. However, the ROI was carefully set based on the consensus of the two experienced radiologists for abdominal

MRI to obtain the most accurate measurement possible. Last, we selected patients with matching clinical data including age, sex, BMI, HbA1c, and the presence or absence of DM in this study. However, hepatic steatosis, alcohol, medication, and ethnicity may also have effects, but we have not considered them this time. In the future, it will be necessary to consider these factors as well.

In conclusion, the PDFF of the pancreas was significantly higher in the IPMN-IC group than in the normal pancreas group and the IPMN group. The observations suggest that the PDFF of the pancreas is associated with the presence of IPMN-IC. Therefore, it is highly recommended that patients with pancreatic fat infiltration be closely monitored regularly for the development of PDAC in a site distant from IPMN.

References

1. Kashiwagi K, Seino T, Fukuhara S, et al. Pancreatic Fat Content Detected by Computed Tomography and Its Significant Relationship With Intraductal Papillary Mucinous Neoplasm. Pancreas. 2018;47(9):1087-92.
2. Yamaguchi K, Kanemitsu S, Hatori T, et al. Pancreatic ductal adenocarcinoma derived from IPMN and pancreatic ductal adenocarcinoma concomitant with IPMN. Pancreas. 2011;40(4):571-80.
3. Baiocchi GL, Molfino S, Frittoli B, et al. Increased risk of second malignancy in pancreatic intraductal papillary mucinous tumors: Review of the literature. World J Gastroenterol. 2015;21(23):7313-9.
4. Omori Y, Ono Y, Tanino M, et al. Pathways of Progression From Intraductal Papillary Mucinous Neoplasm to Pancreatic Ductal Adenocarcinoma Based on Molecular Features. Gastroenterology. 2019;156(3):647-61.e2.
5. Kanno A, Satoh K, Hirota M, et al. Prediction of invasive carcinoma in branch type intraductal papillary mucinous neoplasms of the pancreas. J Gastroenterol. 2010;45(9):952-9.
6. Yamaguchi K, Ohuchida J, Ohtsuka T, Nakano K, Tanaka M. Intraductal papillary-mucinous tumor of the pancreas concomitant with ductal carcinoma of the pancreas. Pancreatology. 2002;2(5):484-90.
7. Kamisawa T, Tu Y, Egawa N, Nakajima H, Tsuruta K, Okamoto A. Malignancies associated with intraductal papillary mucinous neoplasm of the pancreas. World J Gastroenterol. 2005;11(36):5688-90.
8. Kawakami S, Fukasawa M, Shimizu T, et al. Diffusion-weighted image improves detectability of magnetic resonance cholangiopancreatography for pancreatic ductal adenocarcinoma concomitant with intraductal papillary mucinous neoplasm. Medicine (Baltimore). 2019;98(47):e18039.
9. Yagi Y, Masuda A, Zen Y, et al. Pancreatic inflammation and atrophy are not associated with pancreatic cancer concomitant with intraductal papillary mucinous neoplasm. Pancreatology. 2018;18(1):54-60.
10. Kawada N, Uehara H, Nagata S, Tsuchishima M, Tsutsumi M, Tomita Y. Imaging morphological changes of intraductal papillary mucinous neoplasm of the pancreas was associated with its malignant transformation but not with development of pancreatic ductal adenocarcinoma. Pancreatology. 2015;15(6):654-60.
11. Ikegawa T, Masuda A, Sakai A, et al. Multifocal cysts and incidence of pancreatic cancer concomitant with intraductal papillary mucinous neoplasm. Pancreatology. 2018;18(4):399-406.

12. Ingkakul T, Sadakari Y, Ienaga J, Satoh N, Takahata S, Tanaka M. Predictors of the presence of concomitant invasive ductal carcinoma in intraductal papillary mucinous neoplasm of the pancreas. Ann Surg. 2010;251(1):70-5.
13. Kobayashi G, Fujita N, Maguchi H, et al. Natural history of branch duct intraductal papillary mucinous neoplasm with mural nodules: a Japan Pancreas Society multicenter study. Pancreas. 2014;43(4):532-8.
14. Uehara H, Nakaizumi A, Ishikawa O, et al. Development of ductal carcinoma of the pancreas during follow-up of branch duct intraductal papillary mucinous neoplasm of the pancreas. Gut. 2008;57(11):1561-5.
15. Tanaka M, Fernández-Del Castillo C, Kamisawa T, et al. Revisions of international consensus Fukuoka guidelines for the management of IPMN of the pancreas. Pancreatology. 2017;17(5):738-53.
16. Fukui H, Hori M, Fukuda Y, et al. Evaluation of fatty pancreas by proton density fat fraction using 3-T magnetic resonance imaging and its association with pancreatic cancer. Eur J Radiol. 2019;118:25-31.
17. Rebours V, Gaujoux S, d'Assignies G, et al. Obesity and Fatty Pancreatic Infiltration Are Risk Factors for Pancreatic Precancerous Lesions (PanIN). Clinical cancer research : an official journal of the American Association for Cancer Research. 2015;21(15):3522-8.
18. Hori M, Takahashi M, Hiraoka N, et al. Association of pancreatic Fatty infiltration with pancreatic ductal adenocarcinoma. Clin Transl Gastroenterol. 2014;5(3):e53-e.
19. Lesmana CRA, Gani RA, Lesmana LA. Non-alcoholic fatty pancreas disease as a risk factor for pancreatic cancer based on endoscopic ultrasound examination among pancreatic cancer patients: A single-center experience. JGH Open. 2018;2(1):4-7.
20. Fukuda Y, Yamada D, Eguchi H, et al. CT Density in the Pancreas is a Promising Imaging Predictor for Pancreatic Ductal Adenocarcinoma. Ann Surg Oncol. 2017;24(9):2762-9.
21. Majumder S, Philip NA, Takahashi N, Levy MJ, Singh VP, Chari ST. Fatty Pancreas: Should We Be Concerned? Pancreas. 2017;46(10):1251-8.
22. Tomita Y, Azuma K, Nonaka Y, et al. Pancreatic fatty degeneration and fibrosis as predisposing factors for the development of pancreatic ductal adenocarcinoma. Pancreas. 2014;43(7):1032-41.
23. Takahashi M, Hori M, Ishigamori R, Mutoh M, Imai T, Nakagama H. Fatty pancreas: A possible risk factor for pancreatic cancer in animals and humans. Cancer Sci. 2018;109(10):3013-23.
24. Murakami Y, Uemura K, Sudo T, et al. Invasive intraductal papillary-mucinous neoplasm of the pancreas: comparison with pancreatic ductal adenocarcinoma. J Surg Oncol. 2009;100(1):13-8.

25. Tanno S, Nakano Y, Koizumi K, et al. Pancreatic ductal adenocarcinomas in long-term follow-up patients with branch duct intraductal papillary mucinous neoplasms. Pancreas. 2010;39(1):36-40.
26. Ideno N, Ohtsuka T, Kono H, et al. Intraductal papillary mucinous neoplasms of the pancreas with distinct pancreatic ductal adenocarcinomas are frequently of gastric subtype. Ann Surg. 2013;258(1):141-51.
27. Beller E, Lorbeer R, Keeser D, et al. Hepatic fat is superior to BMI, visceral and pancreatic fat as a potential risk biomarker for neurodegenerative disease. Eur Radiol. 2019;29(12):6662-70.
28. Kühn JP, Berthold F, Mayerle J, et al. Pancreatic Steatosis Demonstrated at MR Imaging in the General Population: Clinical Relevance. Radiology. 2015;276(1):129-36.
29. Kromrey ML, Friedrich N, Hoffmann RT, et al. Pancreatic Steatosis Is Associated With Impaired Exocrine Pancreatic Function. Invest Radiol. 2019;54(7):403-8.
30. Aliyari Ghasabeh M, Shaghaghi M, Khoshpouri P, et al. Correlation between incidental fat deposition in the liver and pancreas in asymptomatic individuals. Abdom Radiol (NY). 2020;45(1):203-10.
31. Lesmana CR, Pakasi LS, Inggriani S, Aidawati ML, Lesmana LA. Prevalence of Non-Alcoholic Fatty Pancreas Disease (NAFPD) and its risk factors among adult medical check-up patients in a private hospital: a large cross sectional study. BMC Gastroenterol. 2015;15:174.
32. Zhang Y, Wang C, Duanmu Y, et al. Comparison of CT and magnetic resonance mDIXON-Quant sequence in the diagnosis of mild hepatic steatosis. Br J Radiol. 2018;91(1091):20170587.
33. Lee SS, Park SH. Radiologic evaluation of nonalcoholic fatty liver disease. World J Gastroenterol. 2014;20(23):7392-402.
34. Yokoo T, Bydder M, Hamilton G, et al. Nonalcoholic fatty liver disease: diagnostic and fat-grading accuracy of low-flip-angle multiecho gradient-recalled-echo MR imaging at 1.5 T. Radiology. 2009;251(1):67-76.
35. Hayashi T, Fukuzawa K, Yamazaki H, et al. Multicenter, multivendor phantom study to validate proton density fat fraction and T2* values calculated using vendor-provided 6-point DIXON methods. Clin Imaging. 2018;51:38-42.
36. Serai SD, Dillman JR, Trout AT. Proton Density Fat Fraction Measurements at 1.5- and 3-T Hepatic MR Imaging: Same-Day Agreement among Readers and across Two Imager Manufacturers. Radiology. 2017;284(1):244-54.

Tables

Table 1 Results for comparisons of clinical characteristics among the three groups

	Normal (n = 60)	IPMN (n = 60)	IPMN-IC (n = 12)	*p* value
Age (y)[a]	69.5 ± 8.4	71.0 ± 9.9	74.8 ± 8.6	0.141
Sex				
Male (n = 63)[b]	26 (43.3)	33 (55.0)	4 (33.3)	
Female (n = 69)[b]	34 (56.7)	27 (45.0)	8 (66.7)	0.255
BMI (kg/m^2)[a]	22.9 ± 3.3	22.9 ± 3.9	23.2 ± 1.6	0.657
DM[b]	20 (33.3)	13 (21.7)	4 (33.3)	0.332
HbA1c (%)[a]	6.3 ± 1.0	6.0 ± 0.8	6.5 ± 1.1	0.164

IPMN, intraductal papillary mucinous neoplasm; IPMN-IC, intraductal papillary mucinous neoplasm with concomitant invasive carcinoma; BMI, body mass index; DM, diabetes mellitus; HbA1c, hemoglobin A1c

[a]Data are means ± standard deviation.

[b]Numbers in parentheses are percentages.

Table 2 Results for comparisons of quantitative MRI indices among the three groups

	Normal (n = 60)	IPMN (n = 60)	IPMN-IC (n = 12)	*p* value
SIR-I[a]	1.57 ± 0.43	1.50 ± 0.48	1.63 ± 0.44	0.423
SIR-O[a]	1.51 ± 0.51	1.39 ± 0.54	1.37 ± 0.86	0.153
SIR-T2[a]	1.88 ± 0.47	1.90 ± 0.48	1.78 ± 0.64	0.348
ADC[a] ($\times 10^{-3}$ mm^2/s)	1.50 ± 0.39	1.50 ± 0.30	1.42 ± 0.22	0.684
PDFF[a] (%)	9.09 ± 9.43	9.24 ± 10.7	30.7 ± 20.1	< 0.001

IPMN, intraductal papillary mucinous neoplasm; IPMN-IC, intraductal papillary mucinous neoplasm with concomitant invasive carcinoma; SIR, pancreas-to-muscle (erector spinae muscles) signal intensity ratio; SIR-I, SIR in in-phase imaging; SIR-O, SIR in opposed-phase imaging; SIR-T2, SIR in T2-weighted imaging; ADC, apparent diffusion coefficient; PDFF, proton density fat fraction

[a]Data are means ± standard deviation.

Figure legends

Fig. 1

A 66-year-old woman with fatty liver in the normal pancreas group. Measurements of the region of interest (ROI) are taken in the head of the pancreas on axial in-phase imaging (a), axial opposed-phase imaging (b), axial T2-weighted imaging (T2WI) (c), axial apparent diffusion coefficient (ADC) map (d), and axial multi-echo 3D DIXON (e).

Fig. 2

A 69-year-old man with branch duct type intraductal papillary mucinous neoplasm (IPMN) in the IPMN group. The maximal intensity projection image (MIP) of 3D MR cholangiopancreatography (MRCP) shows a branch duct type IPMN in the head and tail of the pancreas (arrow) (a). Measurements of the ROI are taken in the head of the pancreas on axial in-phase imaging (b), axial opposed-phase imaging (c), axial T2WI (d), axial ADC map (e), and axial multi-echo 3D DIXON (f).

Fig. 3

A 65-year-old woman with histologically proven intraductal papillary mucinous neoplasm with a concomitant invasive carcinoma (IPMN-IC) in the IPMN-IC group. The MIP of 3D MRCP shows a branch duct type IPMN in the tail of the pancreas (arrow) (a). Axial diffusion-weighted image (b) shows a 33-mm-sized mass (arrow) of hyperintensity in the tail of the pancreas. Measurements of the ROI are taken in the head of the pancreas on axial in-phase imaging (c), axial opposed-phase imaging (d), axial T2WI (e), axial ADC map (f), and axial multi-echo 3D DIXON (g). The ROI of the normal pancreas region was set downstream of the tumor to avoid the effect of the tumor on the pancreatic parenchyma.

Fig. 4

Boxplots of the proton density fat fraction (PDFF) of the pancreas in the three groups. The middle bar denotes the median. The cross marks within the box indicate group means. The PDFF of the pancreas was significantly higher in the IPMN-IC group than in the normal pancreas group or the IPMN group ($p < 0.001$ and $p < 0.001$, respectively), and there was no significant difference between the normal pancreas group and the IPMN group ($p = 0.916$).

Figure 1a

Click here to access/download;Figure;figure_1a.tif

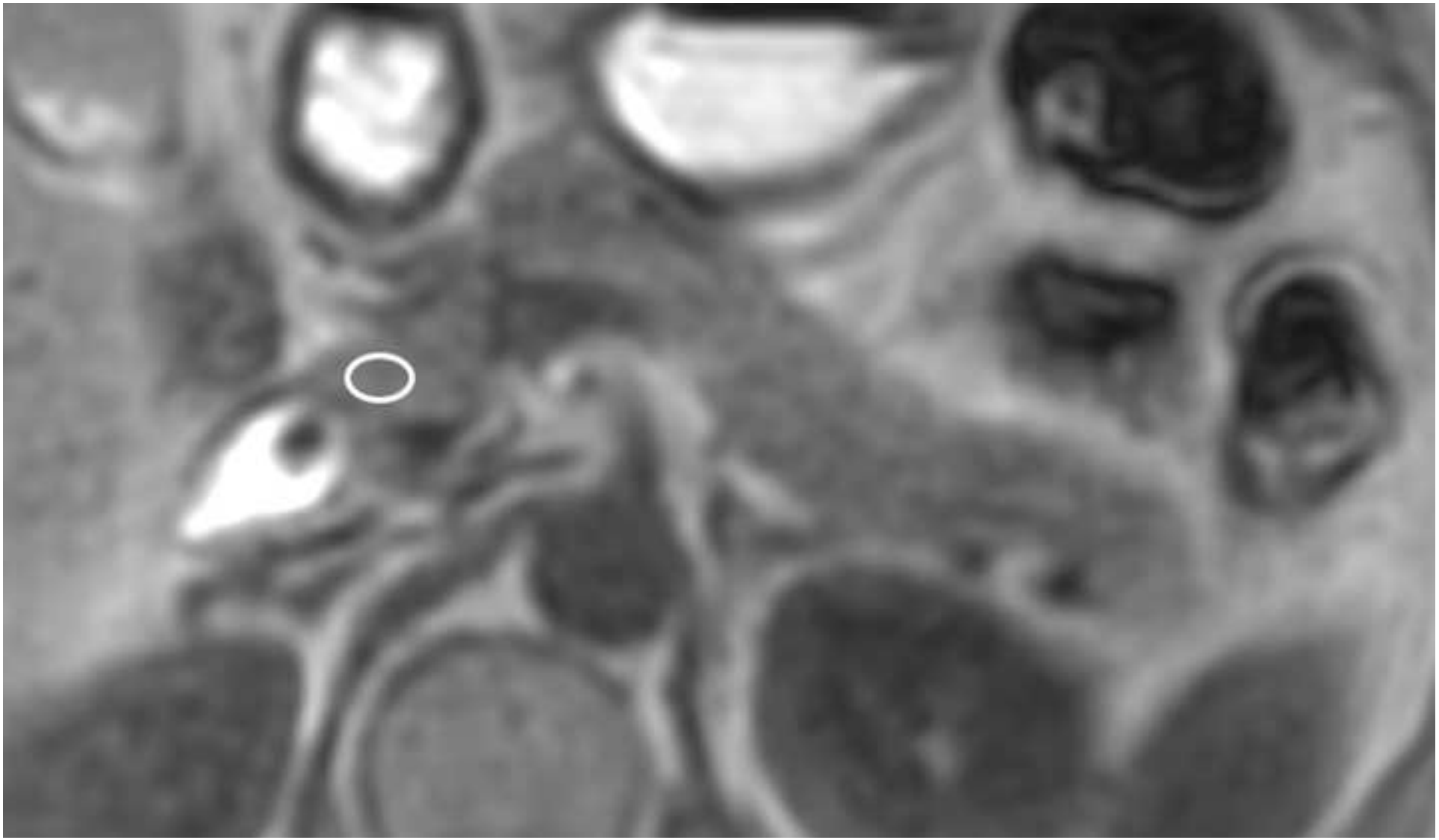

Figure 1b

Click here to access/download;Figure;figure_1b.tif

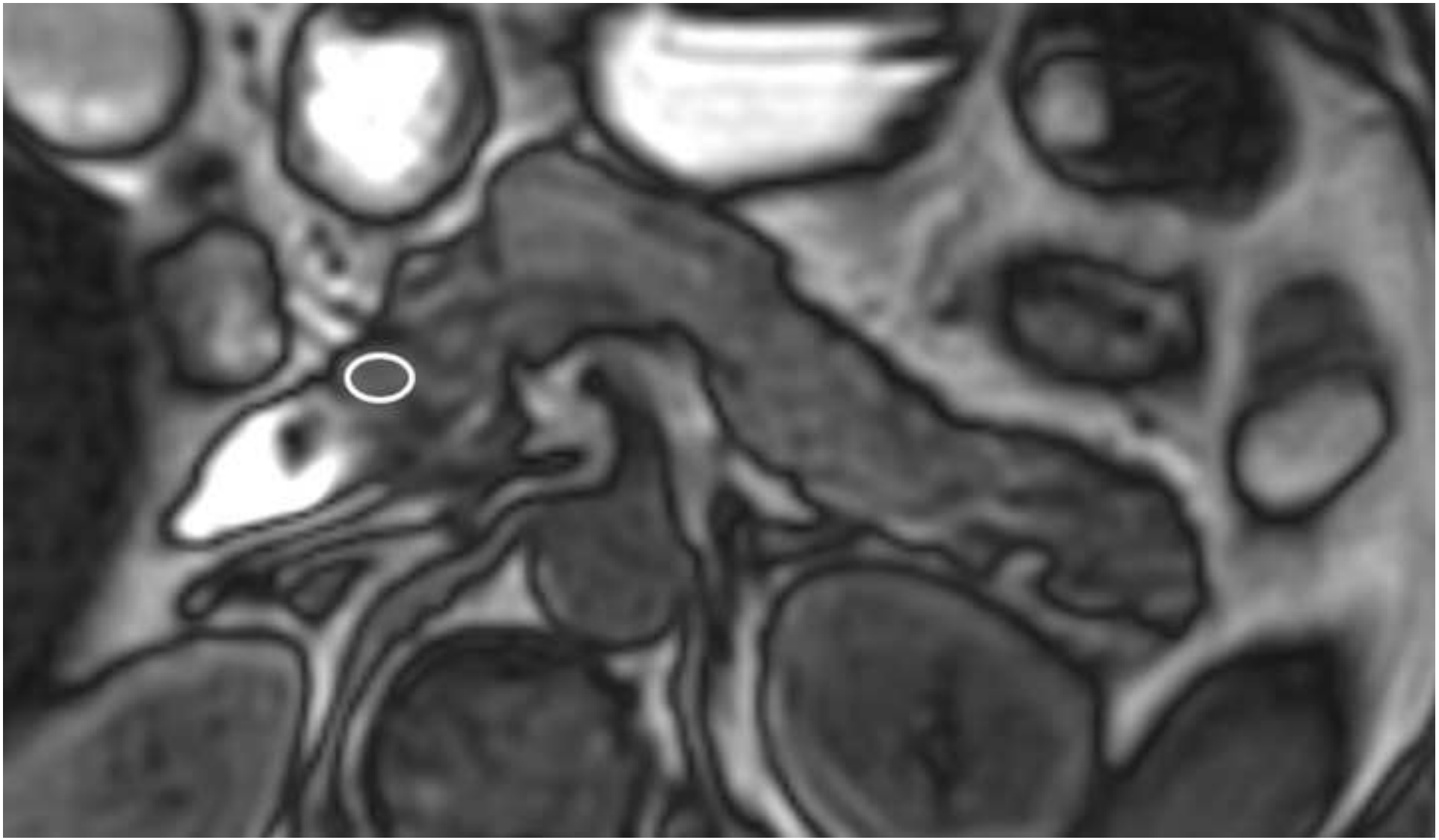

Figure 1c

Click here to access/download;Figure;figure_1c.tif

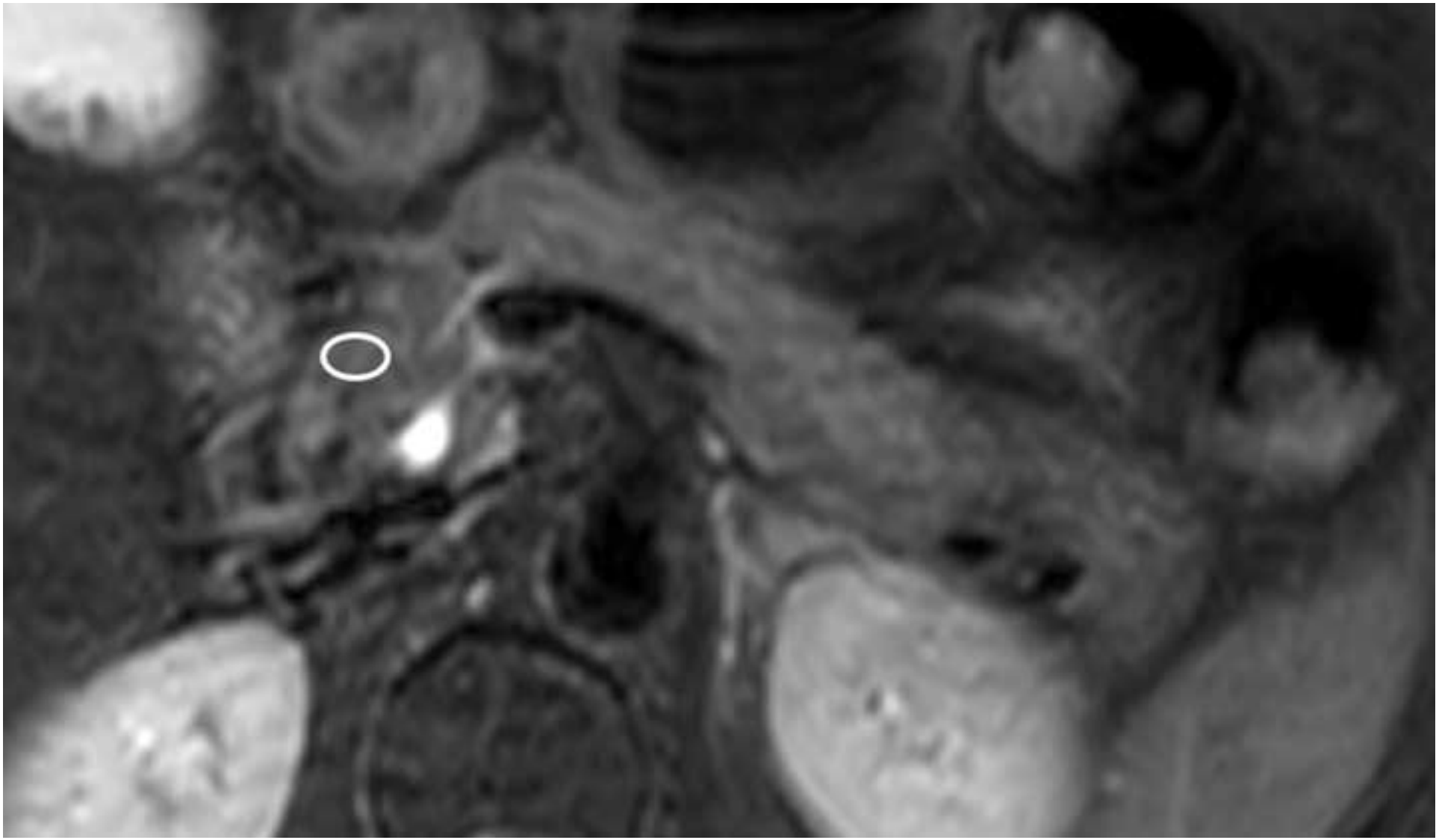

Figure 1d

Click here to access/download;Figure;figure_1d.tif

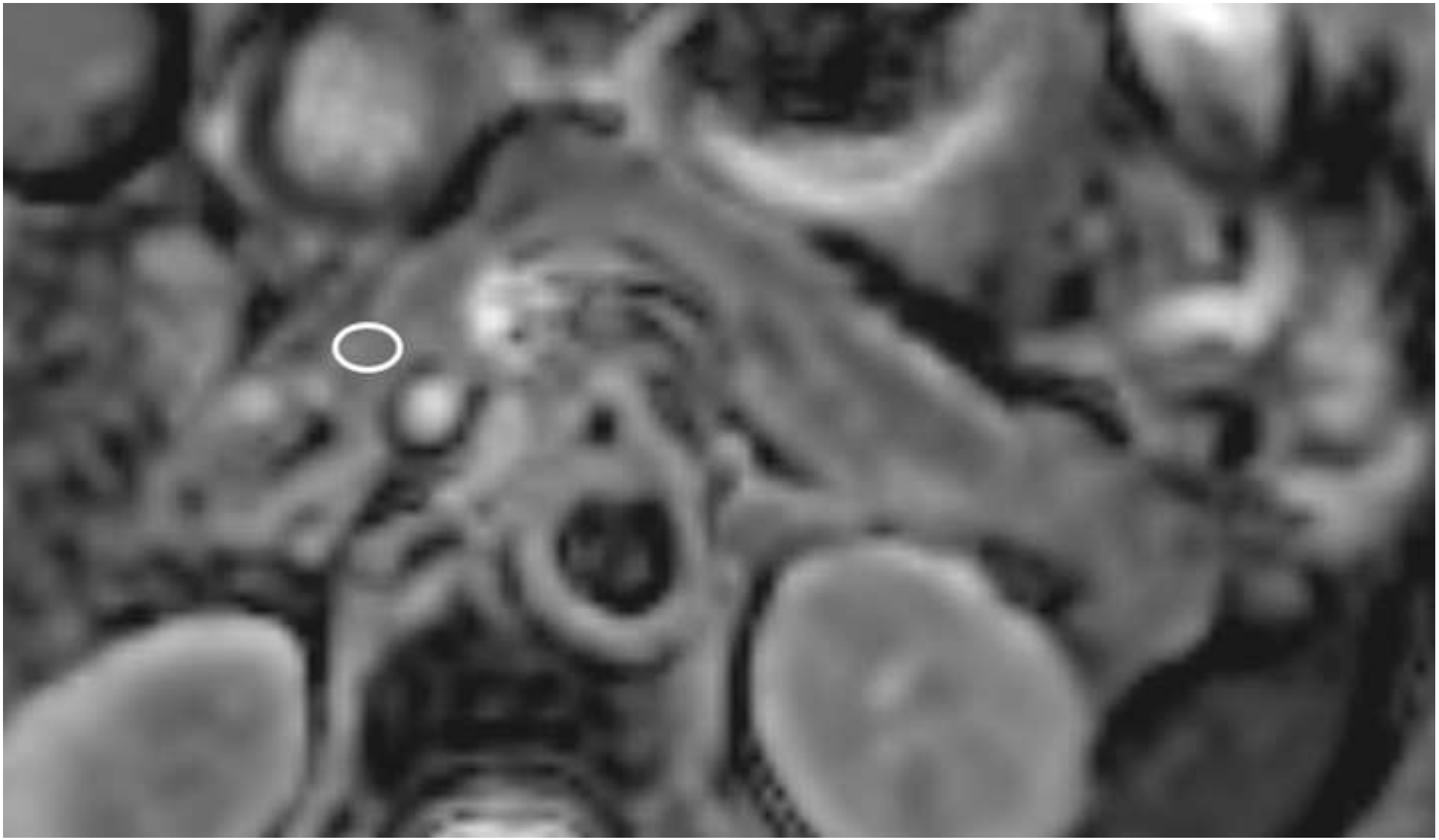

Figure 1e

Click here to access/download;Figure;figure_1e.tif

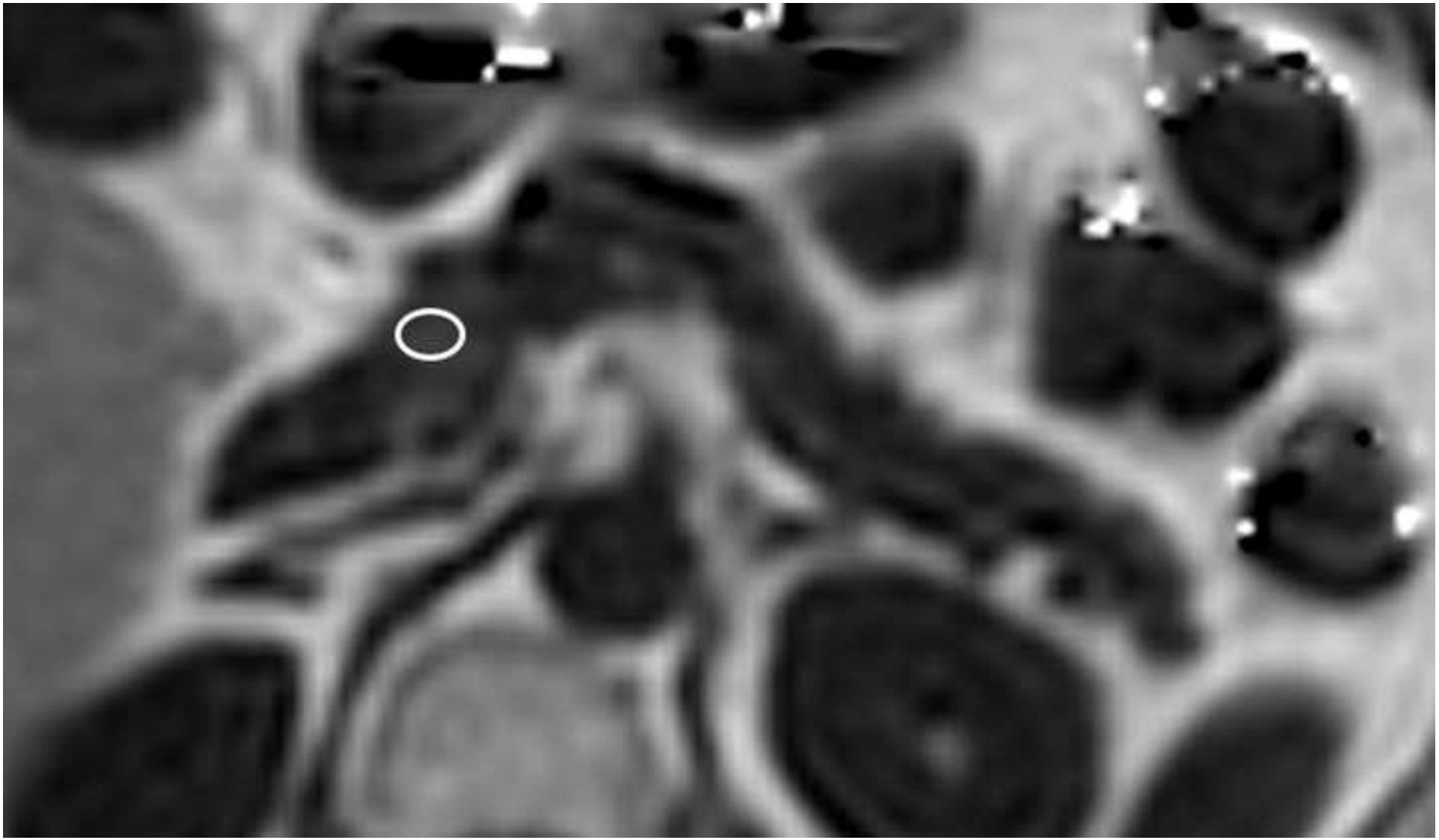

Figure 2a

Click here to access/download;Figure;figure_2a.tif

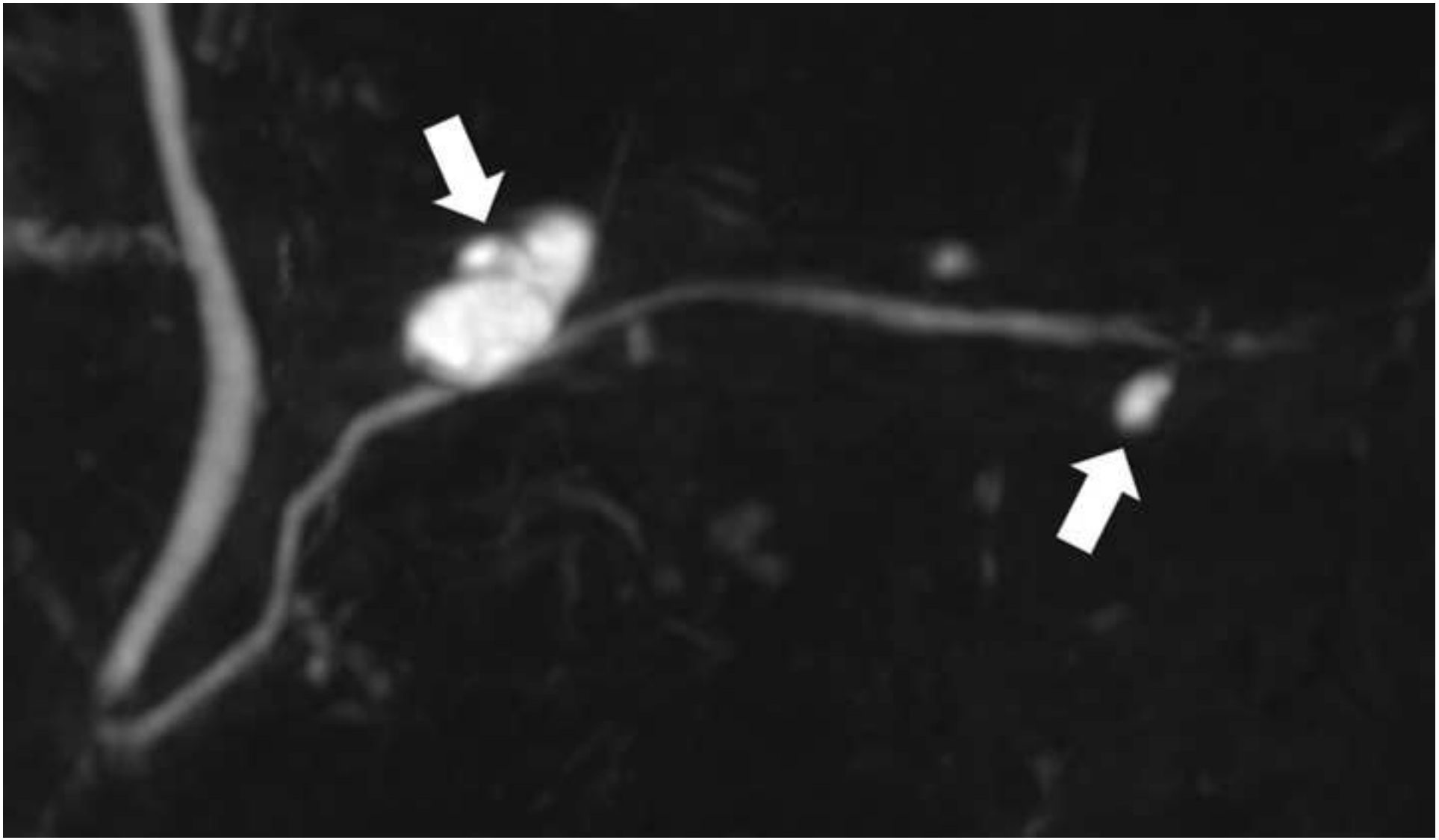

Figure 2b

Click here to access/download;Figure;figure_2b.tif

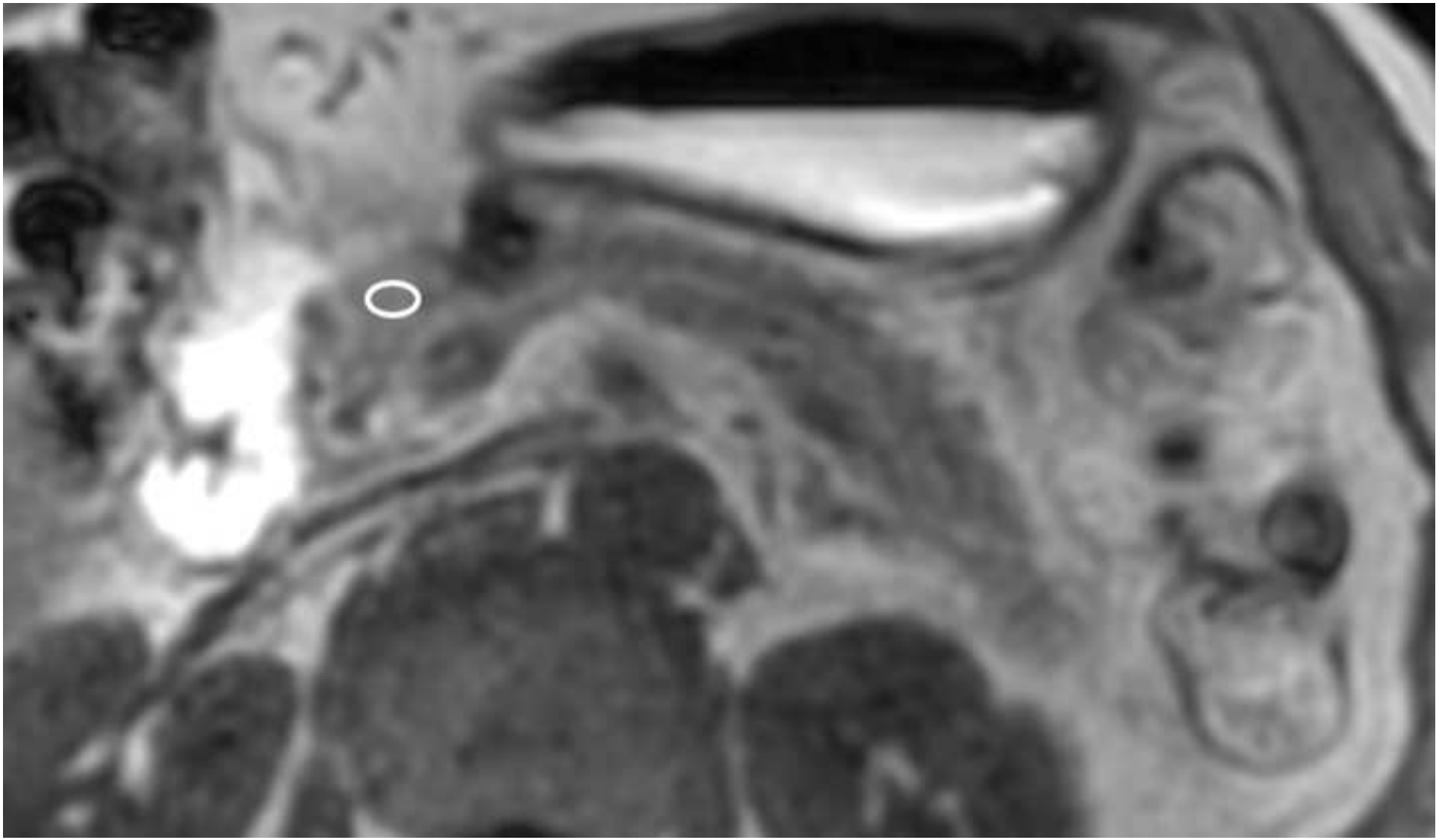

Figure 2c

Click here to access/download;Figure;figure_2c.tif

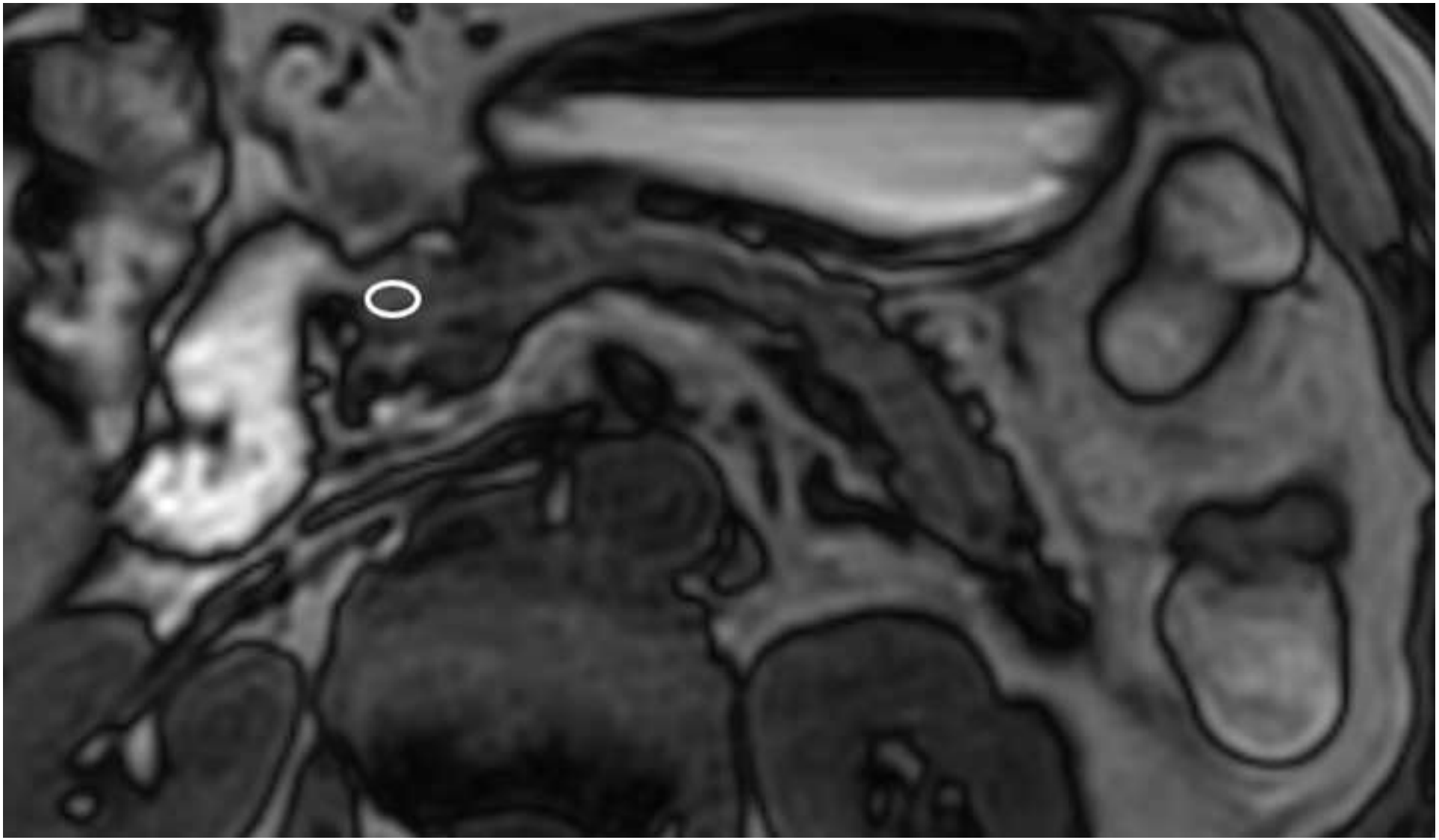

Figure 2d

Click here to access/download;Figure;figure_2d.tif

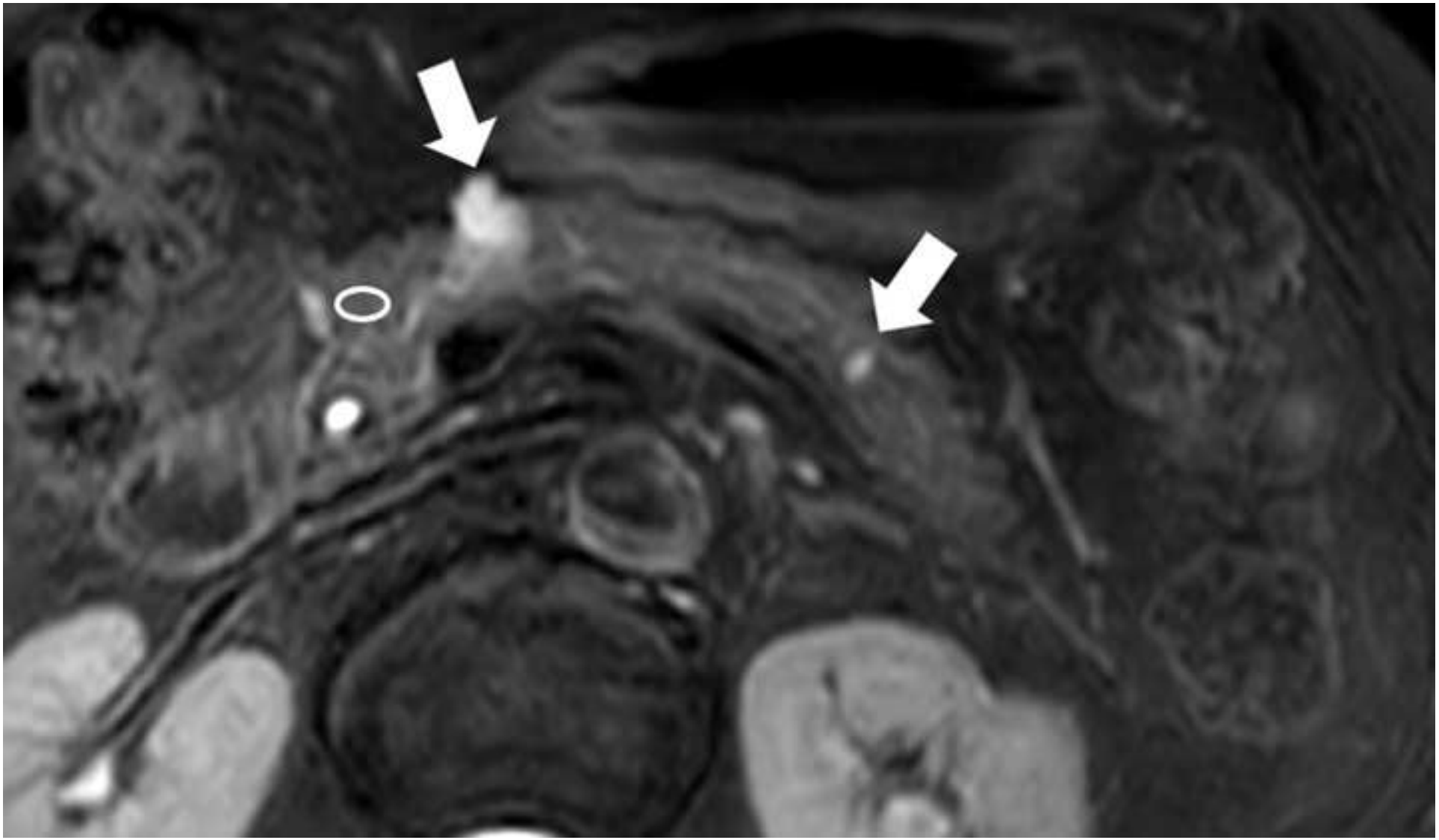

Figure 2e

Click here to access/download;Figure;figure_2e.tif

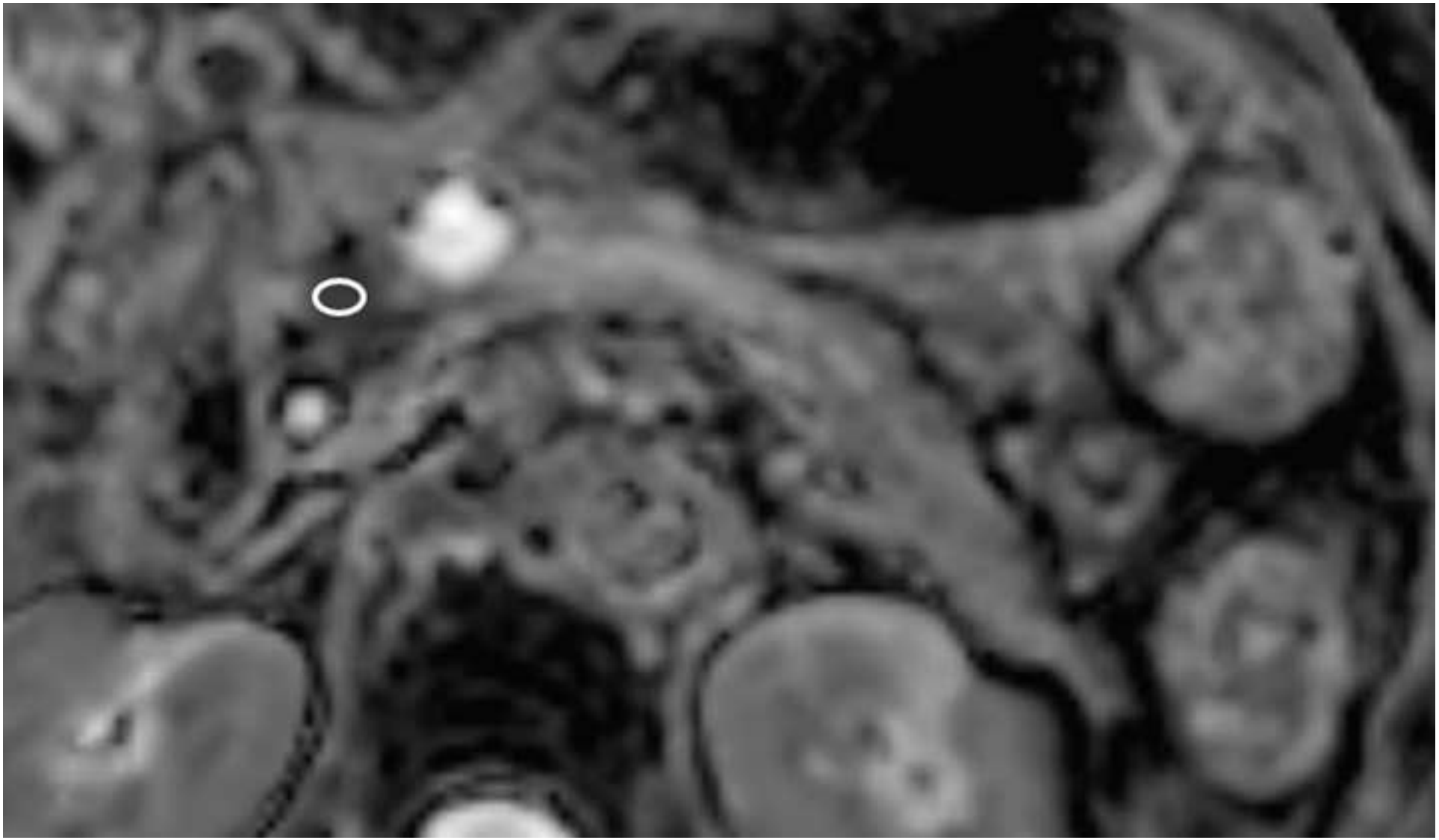

Figure 2f

Click here to access/download;Figure;figure_2f.tif

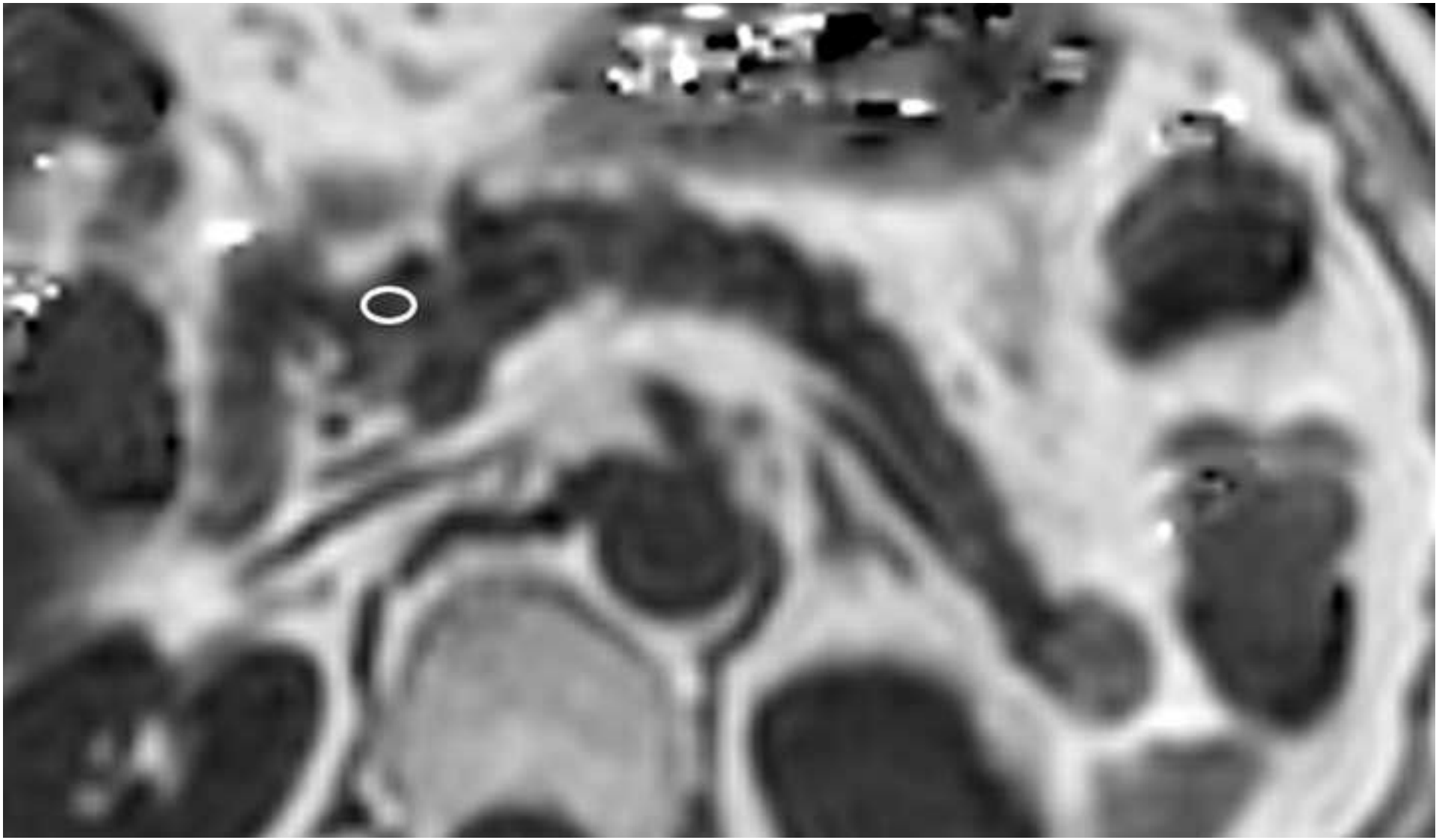

Figure 3a

Click here to access/download;Figure;figure_3a.tif

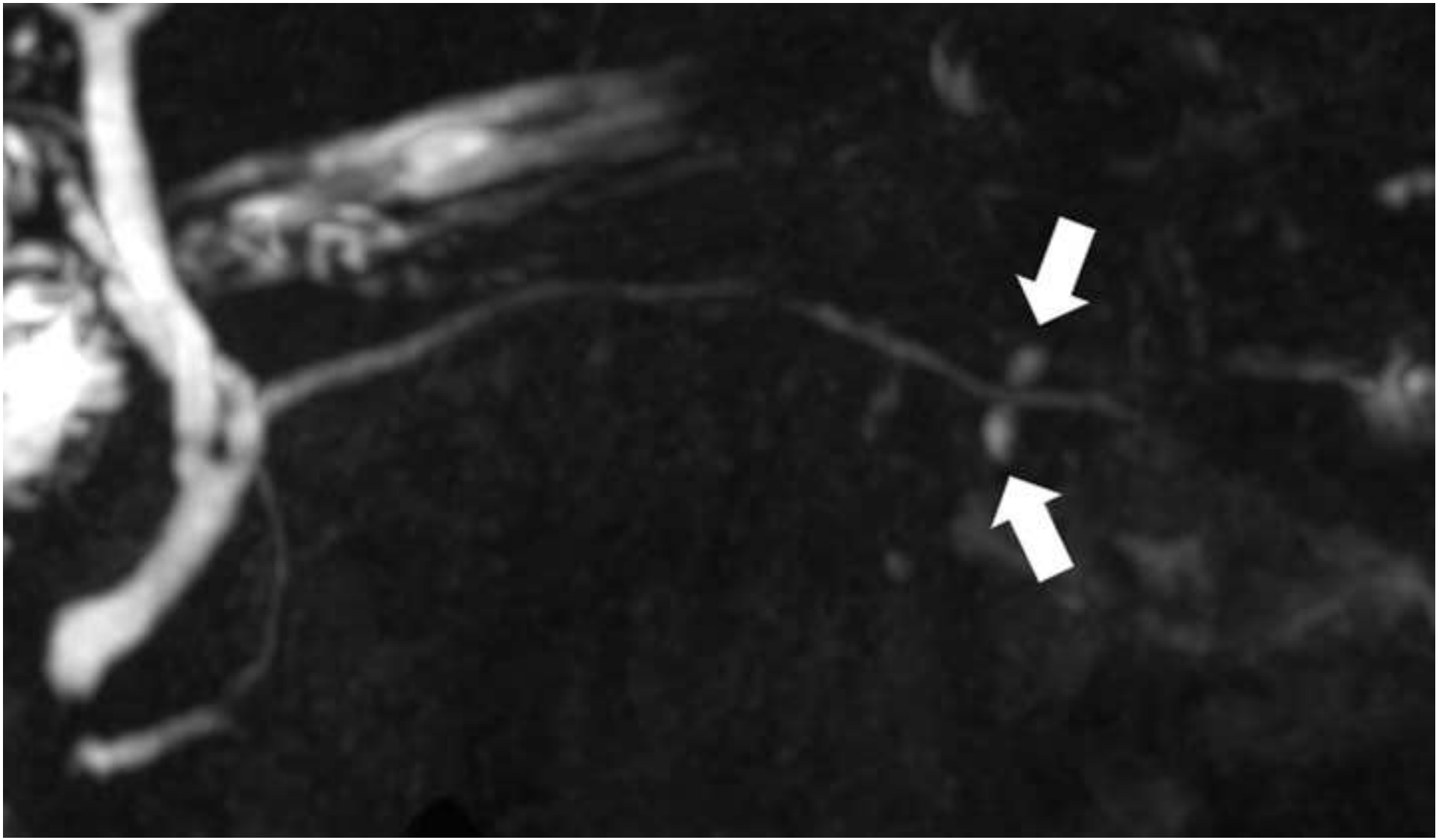

Figure 3b

Click here to access/download;Figure;figure_3b.tif

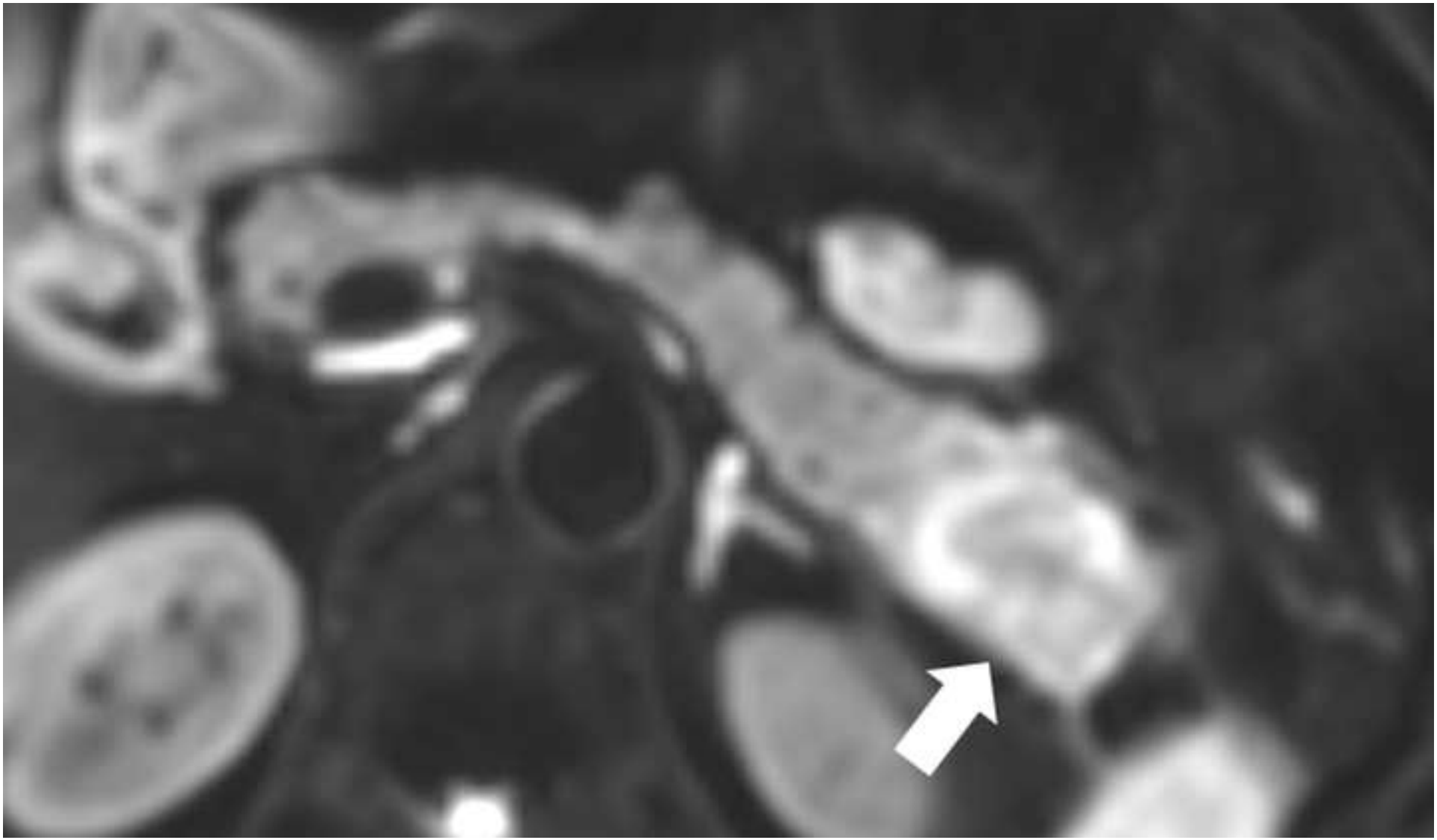

Figure 3c

Click here to access/download;Figure;figure_3c.tif

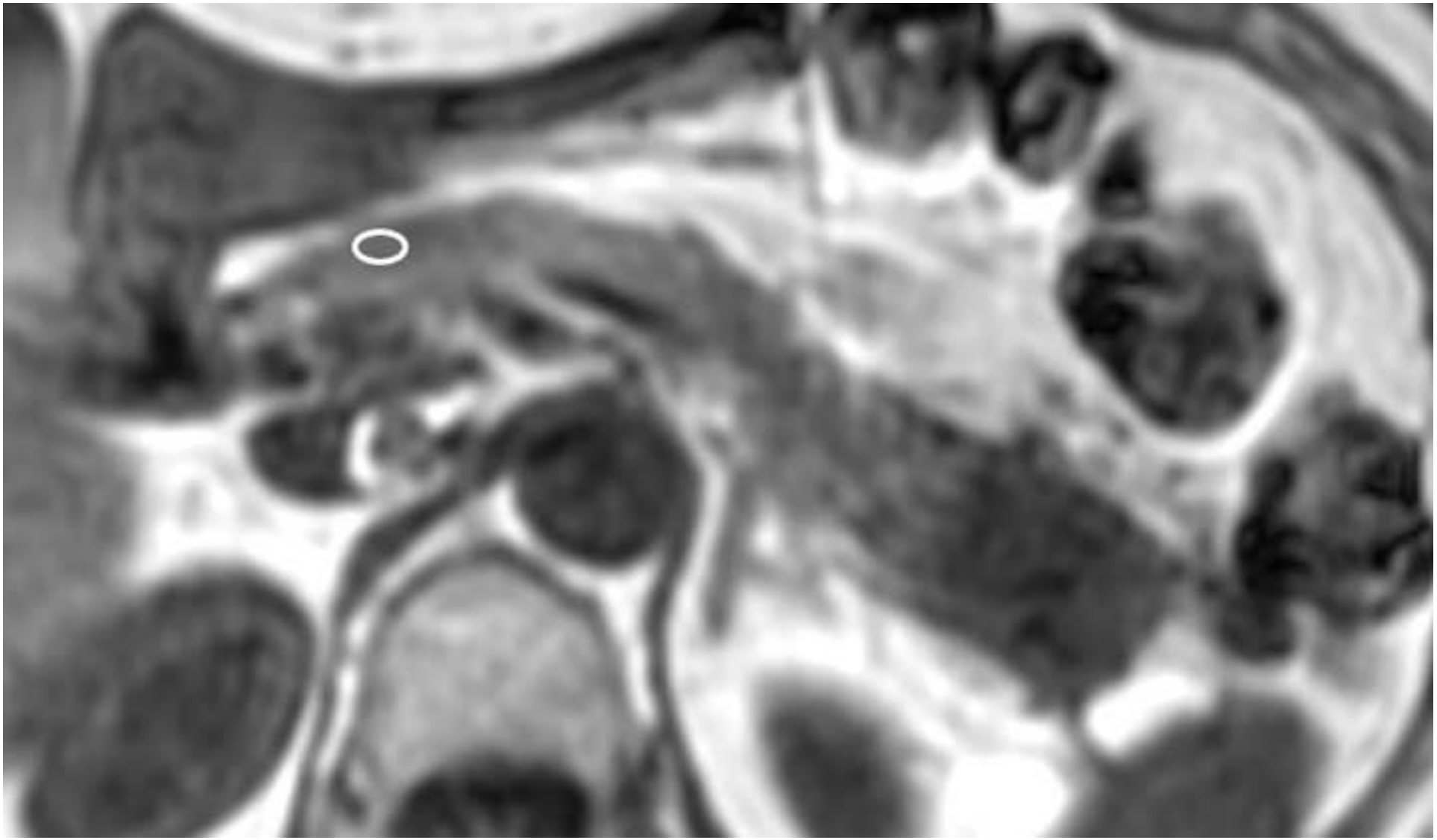

Figure 3d

Click here to access/download;Figure;figure_3d.tif

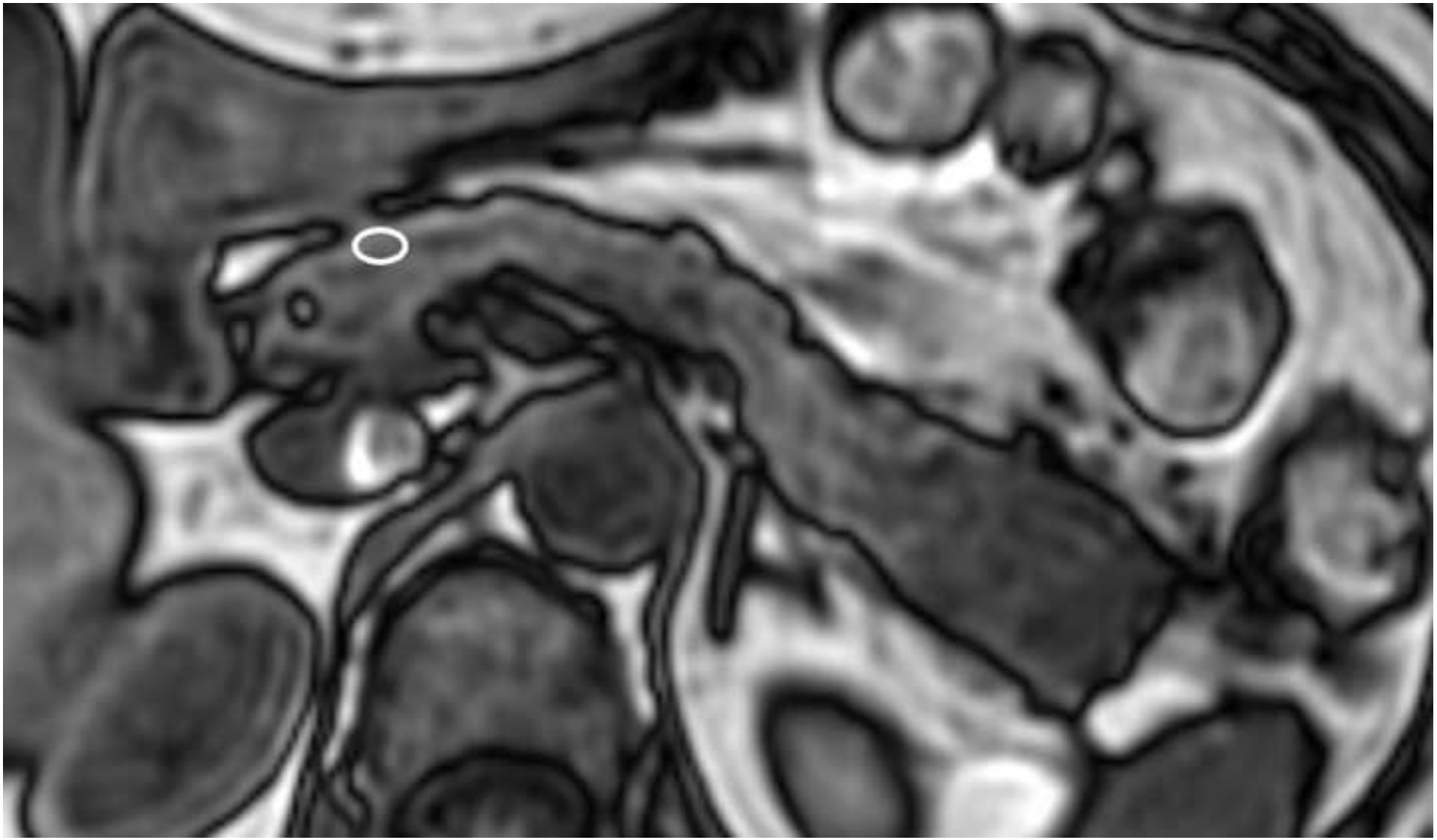

Figure 3e

Click here to access/download;Figure;figure_3e.tif

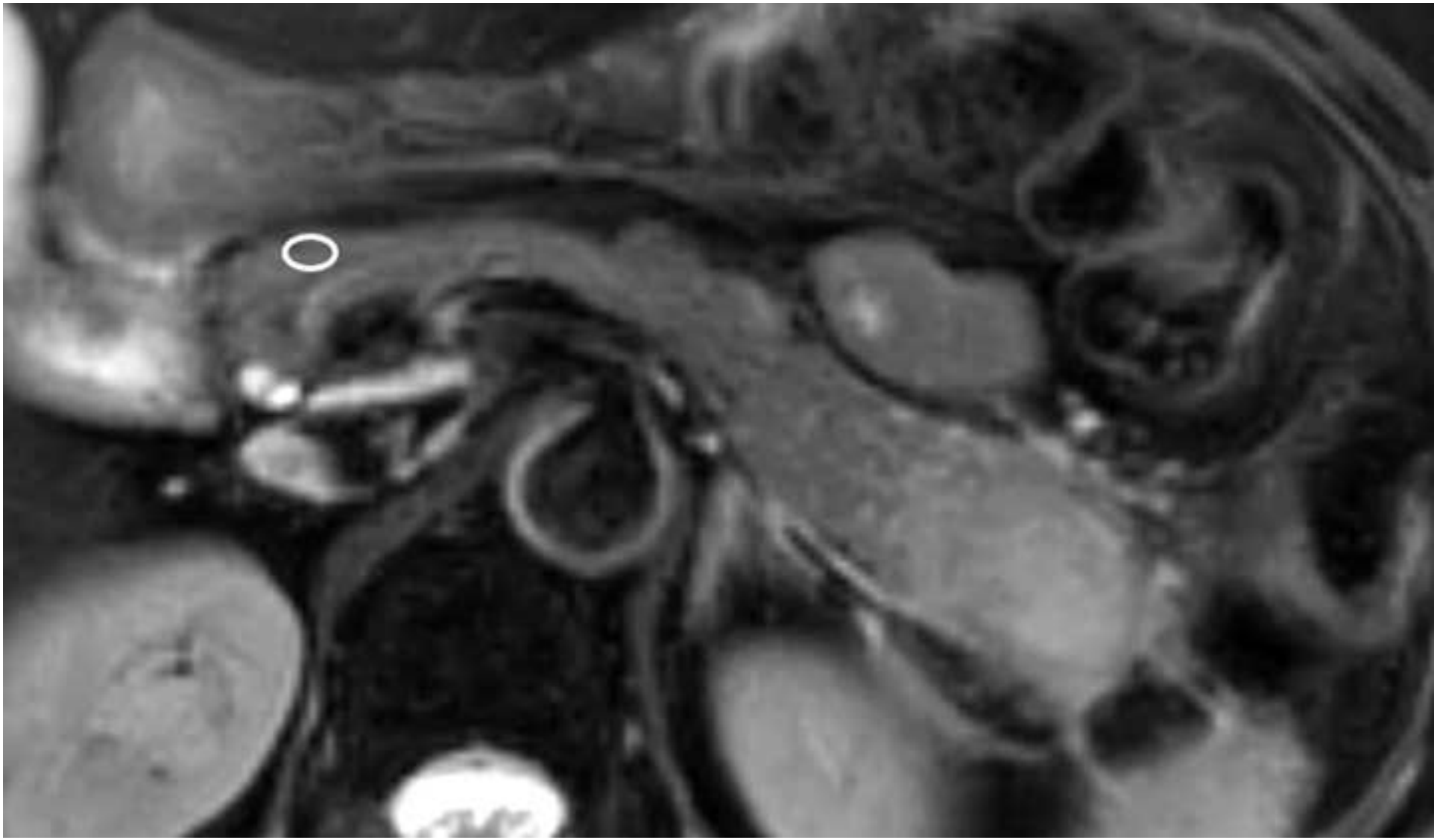

Figure 3f

Click here to access/download;Figure;figure_3f.tif

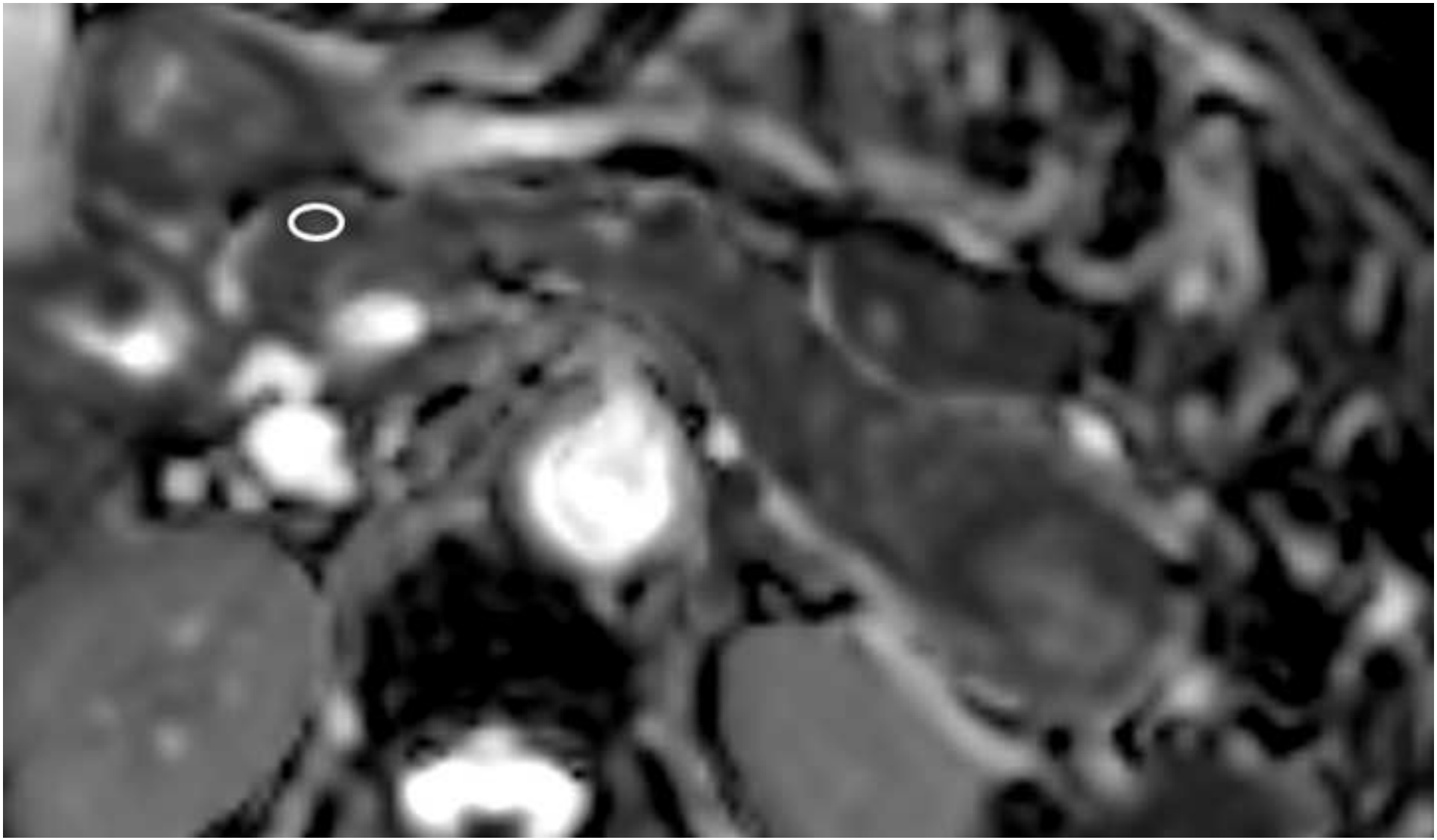

Figure 3g

Click here to access/download;Figure;figure_3g.tif

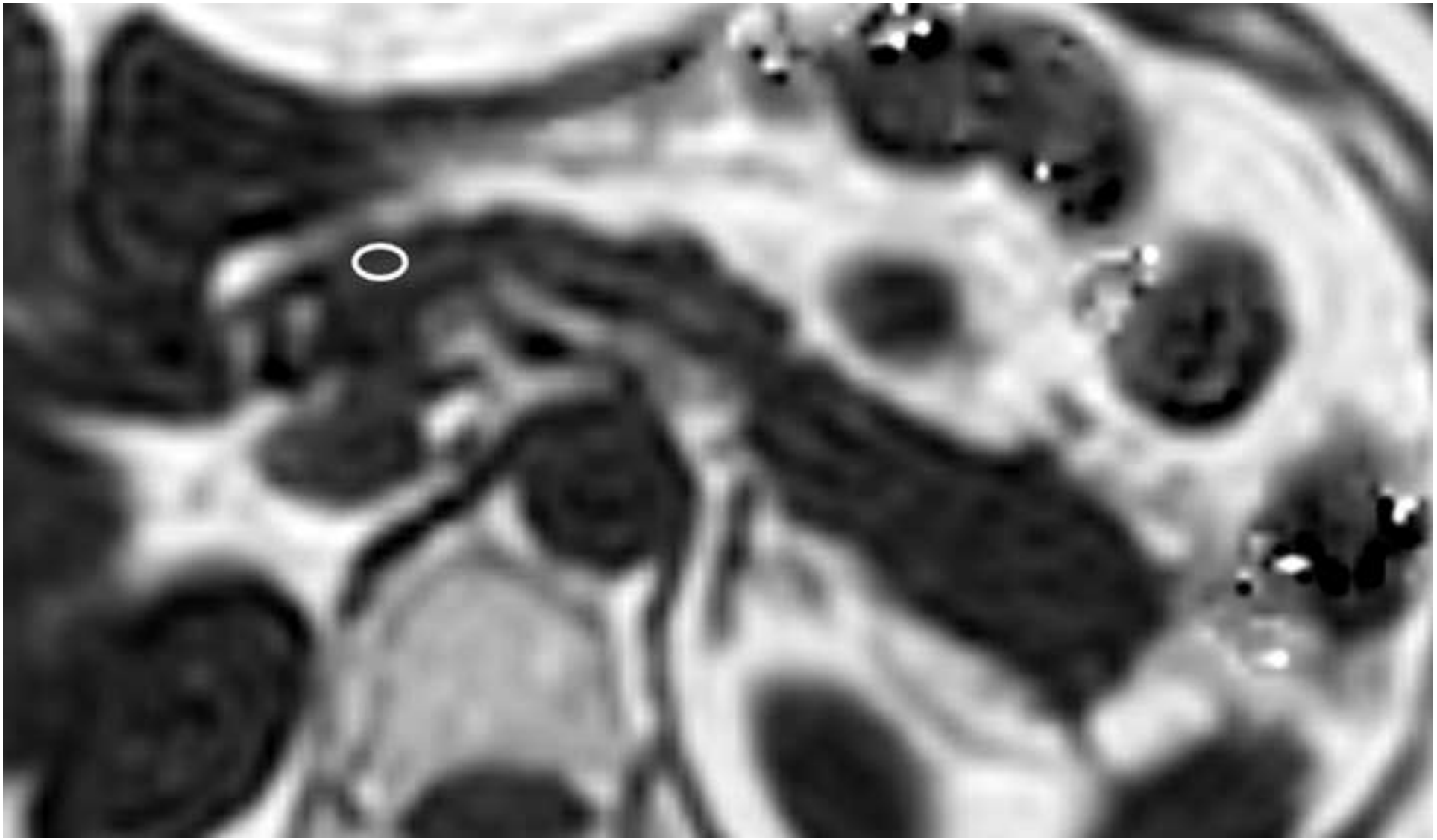

Figure 4

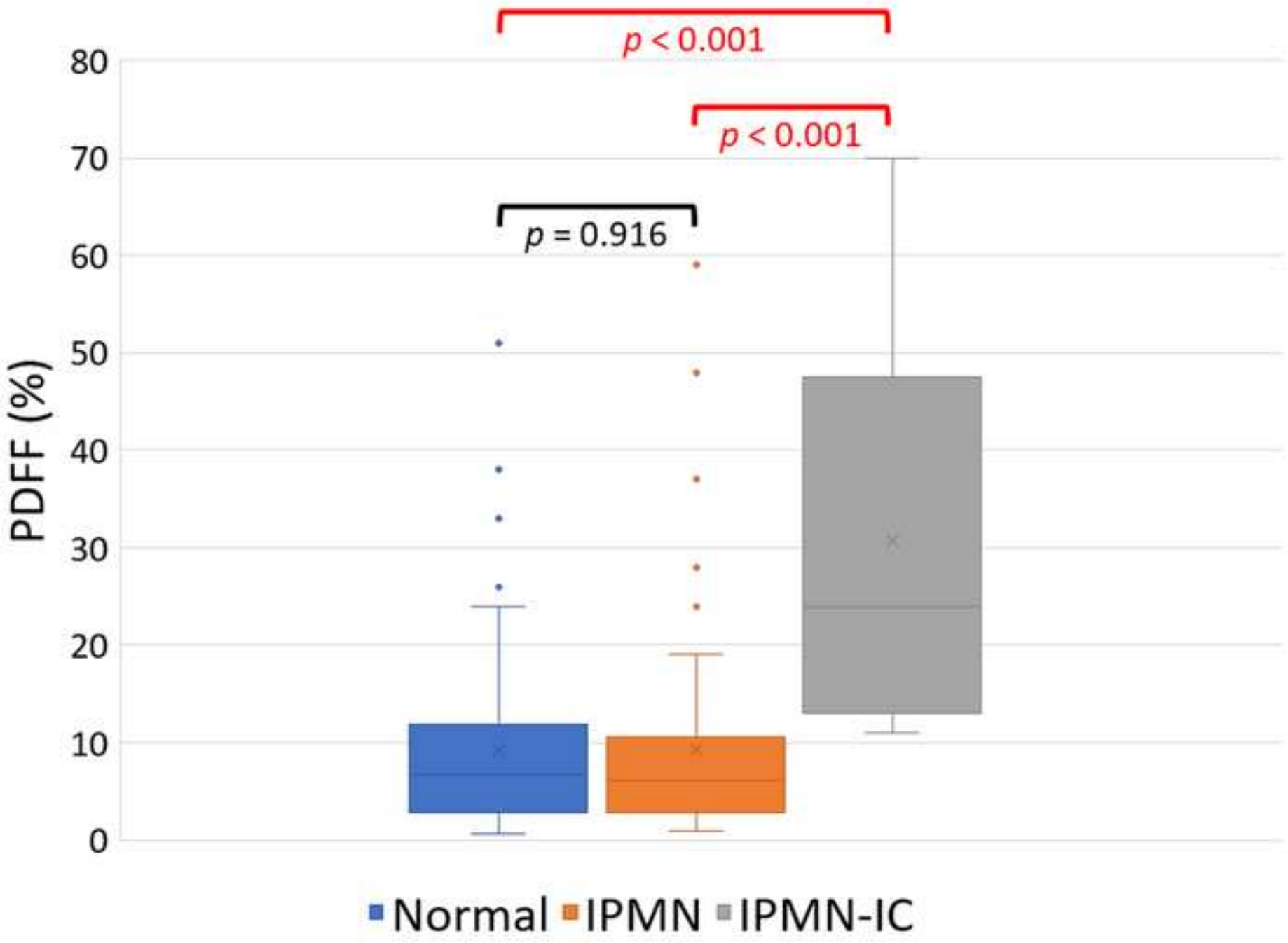

1. ***[Acknowledgements]***

none

2. ***Funding***

The authors state that this work has not received any funding.

Compliance with Ethical Standards

3. ***Guarantor:***

The scientific guarantor of this publication is Tsutomu Tamada.

4. ***Conflict of Interest:***

The authors of this manuscript declare no relationships with any companies, whose products or services may be related to the subject matter of the article.

5. ***Statistics and Biometry:***

One of the authors has significant statistical expertise.

6. ***Informed Consent:***

Only if the study is on human subjects:

Written informed consent was waived by the Institutional Review Board.

7. ***Ethical Approval:***

Institutional Review Board approval was obtained.

8. ***Study subjects or cohorts overlap:***

The subjects included in this study have not been reported.

9. ***Methodology***

Methodology:

- retrospective
- observational
- performed at one institution

Supplementary Material figure 1a

Supplementary Material figure 1b

Supplementary Material figure_1c

Supplementary Material figure_1d

Cover Letter